Bioorganic & Medicinal Chemistry 17 (2009) 905–918

Contents lists available at ScienceDirect

Bioorganic & Medicinal Chemistry

journal homepage: www.elsevier.com/locate/bmc

Selective small molecule inhibitors of the potential breast cancer marker, human arylamine *N*-acetyltransferase 1, and its murine homologue, mouse arylamine *N*-acetyltransferase 2

Angela J. Russell [a,b], Isaac M. Westwood [a], Matthew H. J. Crawford [a,b], James Robinson [a], Akane Kawamura [a], Christina Redfield [c], Nicola Laurieri [a,b], Edward D. Lowe [c,d], Stephen G. Davies [b], Edith Sim [a,*]

[a] Department of Pharmacology, University of Oxford, Mansfield Road, Oxford OX1 3QT, UK
[b] Department of Chemistry, University of Oxford, Chemistry Research Laboratory, Mansfield Road, Oxford OX1 3TA, UK
[c] Department of Biochemistry, University of Oxford, South Parks Road, Oxford OX1 3QU, UK
[d] Laboratory of Molecular Biophysics, Department of Biochemistry, University of Oxford, South Parks Road, Oxford OX1 3QU, UK

ARTICLE INFO

Article history:
Received 28 July 2008
Revised 6 November 2008
Accepted 12 November 2008
Available online 19 November 2008

Keywords:
Arylamine *N*-acetyltransferase
Breast cancer
Rhodanine
Thiazolidin-2,4-dione

ABSTRACT

The identification, synthesis and evaluation of a series of rhodanine and thiazolidin-2,4-dione derivatives as selective inhibitors of human arylamine *N*-acetyltransferase 1 and mouse arylamine *N*-acetyltransferase 2 is described. The most potent inhibitors identified have submicromolar activity and inhibit both the recombinant proteins and human NAT1 in ZR-75 cell lysates in a competitive manner. ^{1}H NMR studies on purified mouse Nat2 demonstrate that the inhibitors bind within the putative active site of the enzyme.

1. Introduction

Arylamine *N*-acetyltransferases (NATs) have been identified as drug- and carcinogen-metabolising enzymes.[1] NAT was initially identified in the late 1950s as a human enzyme that can inactivate, by acetylation, the anti-tubercular drug isoniazid[2] and, subsequently, played an extremely important role in the initial discoveries of genetic polymorphism in drug metabolism,[3] since the loci encoding the NAT isozymes are multi-allelic in humans.[4,5]

NATs are highly conserved throughout the eukaryotic and prokaryotic kingdoms[6] and occur in humans as two isozymes[7,8] human NAT1 and NAT2. NATs catalyse the transfer of an acetyl group from the thio ester of Acetyl-CoA (AcCoA) to a variety of arylamines,[9] arylhydroxylamines[10] and hydrazines[11] (Fig. 1).

This acetylation reaction can lead either to detoxification by *N*-acetylation of arylamine xenobiotics, or to bioactivation by O-acetylation of arylhydroxyamines, by the generation of arylamine acetoxy products capable of decomposing into ultimate carcinogens responsible for DNA adduct formation.[10,12] Kinetic studies of NATs suggest a Ping-Pong Bi–Bi mechanism[9] and the crystal structure from *Salmonella typhimurium*,[13] the first NAT crystal structure to be solved, revealed that the active site Cys residue is part of a catalytic triad, Cys-His-Asp, conserved throughout the NAT family, including *Mycobacterium smegmatis*,[14] *Pseudomonas aeruginosa*[15] and in human NATs for which the structures have been determined.[16]

Human NAT1 and human NAT2 have distinct substrate specificities[17] and tissue distribution,[18,19] despite their high level of homology.[7,8] On the basis of the *C*-terminal sequence identity, substrate specificity and expression profile, human NAT1 is orthologous to mouse Nat2.[17,20] Whilst human *NAT2* is expressed mainly in the liver and intestine, which is consistent with the widely believed view of its role in xenobiotic metabolism, human NAT1 and its homologue mouse Nat2 has a widespread distribution in adult tissues.[7,8,21] It is strongly transcribed in the placenta,[21] early in embryogenesis,[22–24] in embryonic development in the developing neural tube[25] and in folate-sensitive cells contributing to the

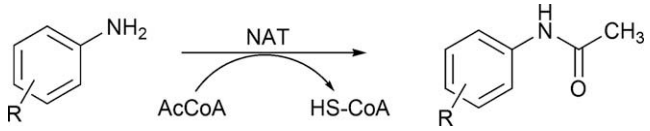

Figure 1. NATs acetylate a large variety of arylamines.

* Corresponding author. Fax: +44 1865 271853.
E-mail address: edith.sim@pharm.ox.ac.uk (E. Sim).

0968-0896/$ - see front matter © 2008 Elsevier Ltd. All rights reserved.
doi:10.1016/j.bmc.2008.11.032

neuroendocrine system.[26] Endogenous roles relating to AcCoA lipid homeostasis[27] or folate metabolism[28] have been proposed for human NAT1. Mouse Nat2 has been identified in vivo to acetylate the folate catabolite *para*-aminobenzoylglutamate (*p*ABAglu).[29] Nevertheless, the exact endogenous role for human NAT1 is still not conclusively identified.

Recent microarray work has confirmed that the human *NAT1* gene is one of the 10 most highly overexpressed genes in ER+ breast cancer cells.[30] Furthermore, the expression of human NAT1 was found to be elevated in invasive ductal and lobular breast carcinomas when compared with normal breast tissue and a strong association of human NAT1 staining with oestrogen receptor-positive (ER+) tumours was demonstrated.[31,32] Also, the active overexpression of human NAT1 in a normal luminal epithelial-derived cell line demonstrated enhanced growth properties relative to control cells.[31] Moreover, the function of folate in cancer biology is intricate, with folate supplements used to prevent tumour formation in normal tissues, although these supplements may accelerate the growth of established tumours, and antifolate drugs have some efficacy as cancer treatments.[33,34]

These results suggest that the complex relationship between human *NAT1* polymorphism and breast cancers and neural tube development may result from a functional link in vivo between NAT1 acetylation activity and folate metabolism.[29] Moreover, it has been demonstrated that the intratumoral dysregulation of xenobiotic-metabolising enzyme expression in breast cancer, including human NAT1, can explain drug resistance, by altered drug metabolism and bioavailability.[32] Among these drugs, tamoxifen, a specific anti-oestrogen compound used to prevent breast cancer cell division in early stages,[35] has also been shown to be an inhibitor of human NAT1,[36,37] as has the chemotherapeutic drug cisplatin.[38] Human NAT1 enzyme activity may also be influenced by some other drugs or oestrogenic agonists or antagonists.[20]

As a result of these studies, understanding the role of the human *NAT1* as a new putative ER+ gene and an attractive potential biomarker in human breast cancer has become crucial. Furthermore, specific activity of human NAT1 in a range of breast cancer cell lines (MCF-7, T47D ZR-75-1), which have been proven to be good models for studying molecular pathways in ER+ breast tumours,[39] were analysed. Of these cell lines assayed, ZR-75-1 cell lysate has a human NAT1 enzyme activity significantly above the others, as human *NAT1* is highly transcribed.[40] In fact, a supplementary activation of human *NAT1* P3 promoter rather than the P1 alternative proximal promoter was observed relative to the other ER+ breast cancer cell lines tested. Whilst ER positivity may be a prerequisite for P3 promoter use, the role of oestrogens in determining which of the alternative human *NAT1* promoters is used is not clear.[40] It has also been demonstrated that both human NAT1 and the oestrogen receptor are down-regulated in tissues in which p53 is mutated.[41] Recent inhibition studies on mouse Nat2, chosen as a model for human NAT1, because of their homology, showed that it is inhibited by endogenous steroids, and steroid mimics such as Bisphenol A.[20]

Breast cancer is the most common cancer in the United Kingdom and worldwide; more than a million women are diagnosed with breast cancer every year, accounting for a tenth of all new cancers and 23% of all female cancer cases. Around 430,000 new cases occur each year in Europe, especially in the most developed countries.[42] Breast cancer is a heterogeneous disease and different breast cancer subtypes can be identified based on gene expression profiling. Current breast cancer therapies, based on Selective Estrogen Receptor Modulators (SERMs) such as tamoxifen or aromatase inhibitors, can be unsuccessful due to intrinsic or acquired resistance to these therapies.[43] Comparing gene expression profiles of tumours either responsive or resistant to tamoxifen therapy is a first step to identify new markers of increased risk or of therapy failure. After profiling gene expression, identification of some unexpected overexpressed genes in breast cancer cells have emerged as new targets for drug discovery. Human NAT1 is one such protein which has emerged as a new diagnostic marker or drug target for breast cancer.

Inhibitors of NATs have recently emerged, both mechanism-based inhibitors,[44] which have found applications in the elucidation of the catalytic mechanism of NATs, and structure-based inhibitors of prokaryotic NATs.[45] The specificity of inhibitors for individual human NAT isoenzymes needs to be addressed. Therefore, in order to identify a series of compounds which are specific for human NAT1, we have carried out a two-stage screening process. Initially we performed a high-throughput screen of our proprietary 5000-member compound library against a panel of five different pure recombinant NAT proteins, including mammalian and non-mammalian NAT enzymes, identifying both broad spectrum NAT inhibitors and inhibitors with specificity for individual NAT isoforms.[45] Hits were subsequently characterised with NAT proteins only available in smaller quantities, but which allowed specificity to be determined. We report on the identification and characterisation of a class of novel NAT isoenzyme-specific inhibitor.

2. Results and discussion

2.1. Recombinant enzymes for high-throughput screening

The human NAT1 enzyme has been generated in a pure form[46,47] and the substrate specificity profile has been demonstrated to be very similar to that of hamster NAT2[17] as well as mouse Nat2.[20] When the initial high-throughput screening was carried out, up to yields of 4-5 mg/L of purified recombinant human NAT1[46,47] and 10-20 mg/L of recombinant hamster Nat2[17] were available. Smaller quantities of human NAT2, mouse Nat2[20] rather than mouse NAT2 and mouse NAT1 also were available for the second phase of more detailed screening of hits from the initial high-throughput screen.

A series of pure recombinant prokaryotic enzymes have also been produced in substantial quantities and their individual substrate specificities have been characterized.[13–15,48] The stability and storage conditions of each of the pure recombinant enzymes has been established and, together with the data on their characterization, provides a good panel for screening and controls for isoenzyme specificity.

2.2. Inhibitors identified by high-throughput screening

We screened our library of 5000 drug-like[49] small molecules against a panel of five NAT enzymes from both prokaryotes and eukaryotes. This library has been designed and selected to cover a wide range of biological space, to omit any known cytotoxic agents and to ensure that selected structures are amenable to both resynthesis and rapid diversification.[45]

Recombinant NAT enzymes from the following bacteria were used in the screen: *P. aeruginosa*,[15] *M. smegmatis*[14] and *S. typhimurium*.[13,48] The eukaryotic NATs used were human NAT1 and hamster NAT2.[17] The assay method previously described by Brooke and colleagues was used,[11] with some modifications for automation purposes. In the assay reaction, free coenzyme A is produced, and this is reacted with Ellman's reagent [5,5′-dithio-bis(2-nitrobenzoic acid)] to produce 5-thio-2-nitrobenzoic acid, which was detected spectrophotometrically with a 96-well plate reader.

The compound library was screened against each enzyme, with two different substrates, such that for each protein a substrate with differing K_m and V_{max} values would be used to cover possible endogeneous substrates where none was yet identified. The library was screened at a final concentration of approximately 30 μM

against the bacterial NAT enzymes with the substrates 5-aminosalicylic acid (5-AS) and isoniazid (INH)[11,14,50] and against the mammalian enzymes with the substrates 5-AS and *p*-aminobenzoic acid (pABA).[17]

Hit selection was assessed as follows: specific inhibitors of the eukaryotic NAT proteins were defined as those which inhibited both human NAT1 and hamster NAT2 (with both substrates) more than 50% at 30 μM but which did not inhibit any of the prokaryotic NAT enzymes more than 20% at the same concentration. This was also coupled with *Z*-score analysis to compensate for any systematic errors related to plate position. The strategy used was designed to maximise the hit rate, minimising both false-positive and false-negative results. In this manner, 50 compounds were identified as active, showing specificity for the eukaryotic NAT proteins, and were subjected to a secondary screen to allow their prioritisation.

To develop a tool to probe the role of human NAT1 in disease, compounds with selectivity for human NAT1 over its paralogue, human NAT2, which is known to have a key role in drug metabolism, were of interest. Similarly, it was desired for the compounds to be used as tools to probe the role of the orthologous gene product in mouse, as an important disease model, and compounds which were also inhibitors of mouse Nat2 were therefore vital to investigate. Thus, the 50 compounds identified as selective inhibitors of human NAT1 and hamster NAT2 from the initial screen were subjected to a secondary screen against a further panel of NAT enzymes, including pure recombinant enzymes which were available in smaller quantities. The enzymes for the secondary screen were human NAT1 (HNAT1), human NAT2 (HNAT2),[47] mouse Nat1 (MNat1), mouse Nat2 (MNat2) and two prokaryotic NATs for comparison, from *P. aeruginosa*[15] (PANAT) and *Mycobacterium marinum* (MMNAT).[51] Selected results are shown in Table 1. Compounds were selected from the secondary screen for further study that showed selectivity for HNAT1 and MNat2 over their orthologues, HNAT2 and MNat1.

Next, the six most active compounds (**1**, **3**–**5**, **7** and **8**) with selectivity for human NAT1 and mouse Nat2 over their orthologs were further investigated for their effects on the inhibition of NAT activity in ZR-75 breast cancer cell lysates using pABA, a human NAT1-specific substrate. For comparison, two NAT inhibitors (**10** and **11**) which specifically inhibited the prokaryotic enzymes were also included in the assay (Fig. 2). As anticipated, the two prokaryote-specific NAT inhibitors did not inhibit either purified recombinant mouse Nat2 or human NAT1 or inhibit NAT activity in ZR-75 cell lysates. Of the six human NAT1/mouse Nat2-selective inhibitors, only two, compounds **1** and **5** also inhibited NAT activity in ZR-75 cell lysates. The reduced activity of the remaining compounds **3**, **4**, **7** and **8** compared with their activity when tested with pure recombinant human Nat1 may be a consequence of increased binding of these species to other proteins within the lysate, thus significantly reducing their effective concentration in vitro. Compounds **3**, **4**, **7** and **8** were therefore not pursued further in this study.

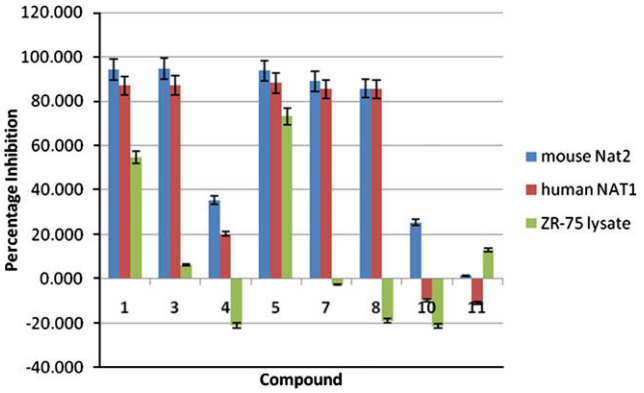

Figure 2. Percentage inhibition of six selected compounds from the secondary screen (**1**, **3**–**5**, **7** and **8**) along with two inhibitors showing selectivity for prokaryotic NATs (**10** and **11**) at 30 μM concentration against the recombinant mouse Nat2 recombinant human NAT1 and ZR-75 cell lysate with PABA as substrate.

Compound **5** was initially selected for further studies. Early efforts were therefore directed towards the synthesis and in vitro evaluation of **5** first to validate its inhibitory activity against human NAT1 and mouse Nat2, and subsequently to optimise its activity through the synthesis of a range of structural analogues.

2.3. Validation of rhodanine (5)

The synthesis of (*Z*)-5-(4′-hydroxy-3′,5′-diiodobenzylidene)-2-thioxothiazolidin-4-one (**5**) was carried out according to a modification of the conditions described by Unangst et al.[52] 2-Thioxothiazolidin-4-one and 4-hydroxy-3,5-diiodobenzaldehyde were reacted together in the dark, under an atmosphere of N_2 to give **5** in 94% yield as a single diastereoisomer. The (*Z*)-configuration within **5** was assigned by analogy to previously reported data on related species (Scheme 1).[53]

Having confirmed the activity of the authentic sample of **5** (Table 1), the IC_{50} values were next determined against human NAT1 and NAT1 in ZR-75 cell lysate and were determined to be

Table 1
Selected data from the secondary screen

	ID	HNAT1	MNat2	HNAT2	MNat1	MMNAT	PANAT
Eukaryotic NAT-selective inhibitors	**1**	98 ± 2	95 ± 1	−43 ± 16	−2 ± 6	64 ± 8	8 ± 9
	2	19 ± 5	55 ± 9	53 ± 12	37 ± 8	9 ± 3	18 ± 13
	3	94 ± 3	82 ± 7	−16 ± 14	11 ± 10	−8 ± 4	−2 ± 15
	4	93 ± 1	100 ± 4	−20 ± 14	10 ± 4	80 ± 1	37 ± 7
	5	89 ± 2	91 ± 2	19 ± 13	10 ± 4	89 ± 2	94 ± 1
	5[a]	86 ± 4	104 ± 5	46 ± 2	N.D.	40 ± 2	52 ± 3
	6	100 ± 2	99 ± 8	−23 ± 13	46 ± 3	16 ± 7	1 ± 18
	7	99 ± 1	96 ± 1	−35 ± 9	35 ± 13	−2 ± 18	11 ± 13
	8	95 ± 1	62 ± 4	0 ± 25	6 ± 4	14 ± 7	58 ± 5
	9	72 ± 36	76 ± 5	4 ± 9	29 ± 5	15 ± 4	13 ± 14
Prokaryotic NAT-selective inhibitors	**10**	16 ± 6	0 ± 6	73 ± 2	51 ± 10	98 ± 1	99 ± 1
	11	10 ± 19	−1 ± 15	82 ± 6	53 ± 13	100 ± 0	87 ± 3
	12	−2 ± 4	−7 ± 10	78 ± 2	56 ± 7	97 ± 3	100 ± 3

Percentage inhibition at 30 μM inhibitor versus HNAT1, MNat2, HNAT2, MNat1, MMNAT and PANAT using 5-AS as substrate.

[a] Resynthesised sample. N.D., not determined. It was noted that some compounds appeared to be inhibitors of PANAT in this second more discriminating screen including **4**, **5** and **8**, presumably indicating these data were false-positives in the primary screen. However, the main criterion for pursuing a compound was selectivity against the mammalian homologues and thus, **1**, **3**–**5**, **7** and **8** were pursued.

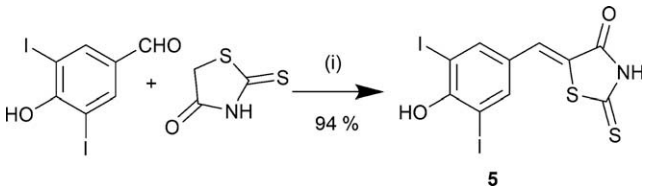

Scheme 1. Reagents and condition: (i) NH_4OAc, Toluene, Δ, 24 h.

0.33 ± 0.06 and 0.138 ± 0.039 μM, respectively (Fig. 3, left and middle panels, respectively). Kinetic analyses were also undertaken, indicating that **5** is a competitive inhibitor of human NAT1 (Fig. 3, right panel). Given the relatively small size of **5**, with a heavy atom count of just 17, the IC_{50} value of 0.33 ± 0.06 μM against human NAT1 is a remarkably low value, corresponding to a ligand efficiency[54] of 0.52 kcal mol^{-1}. This is a high value for ligand efficiency, where 0.3 kcal mol^{-1} is a typical cutoff for progression from screening to hit-to-lead development of a hit from a fragment screen.[54] This reaffirms the high affinity of **5** for human NAT1, and indicates that this compound is a suitable starting point for future development of potent human NAT1 inhibitors.

To develop a small molecule tool to probe the role of NAT1 in a cellular context, a series of analogues of **5** were next prepared to investigate structure–activity relationships (SARs), with the aim of improving its inhibitory potency.

2.4. SAR analysis

Early structure–activity investigations around compound **5** revealed that NAT inhibitory activity was diminished when the parent heterocycles, rhodanine, *N*-amino rhodanine, *N*-methyl rhodanine or thiazolidine-2,4-dione were employed. Several series of analogues of **5** were thus prepared varying systematically at the heterocyclic core and the aryl aldehyde condensation partners. Subsequently the use of aliphatic aldehyde and ketone derived condensation products was explored. Condensation was accomplished in a parallel fashion by refluxing the requisite heterocycle and aldehyde or ketone in toluene or ethyl acetate in the presence of ammonium acetate over 3–15 h, affording the corresponding condensation products in 16 to >99% yield and excellent purity (Scheme 2).

The condensation products were then evaluated for their inhibitory activity at a range of concentrations against the recombinant human NAT1 promoted acetylation of PABA. The extent of inhibition was determined by measuring the rate of hydrolysis of acetyl CoA using 5,5′-dithio-bis(2-nitrobenzoic acid), as described above. IC_{50} values are depicted in Tables 2–5.

The effect of varying the aryl substituent whilst keeping the rhodanine core constant was first investigated (Table 2). In most cases, NAT inhibitory activity was highest with an *ortho*-substituent on the aryl ring, with activity diminishing in the corresponding *meta*- or *para*-substituted regioisomers, with the most active analogues identified as *ortho*- and *meta*-hydroxy-substituted derivatives **15** (IC_{50} 1.1 μM) and **14** (IC_{50} 0.6 μM).

The most potent derivatives were subsequently screened for selectivity against mouse Nat2 (using pABA as substrate), PANAT and MMNAT (using INH as substrate) (Fig. 4). In most cases, the compounds still showed specificity for the two eukaryotic NATs tested, with PANAT or MMNAT showing typically less than 40% inhibition in each case. Several examples showed similar levels of inhibitory activity against human NAT1 and mouse Nat2, consistent with the previously observed similarities in the substrate selectivity profiles.[17,20] Further SAR studies were therefore conducted on mouse Nat2 as a good model for predicting inhibitory activity against human NAT1.

The effect of varying the heterocyclic core was next explored (Table 3). Incorporation of an *N*-methyl substituent (**27**) was observed to lead to a decrease in NAT inhibitory activity, whereas an *N*-amino substituent was observed to lead to a slight increase in activity. The thiazolidine-2,4-dione-derived species **29** showed a 2-fold reduction in activity.

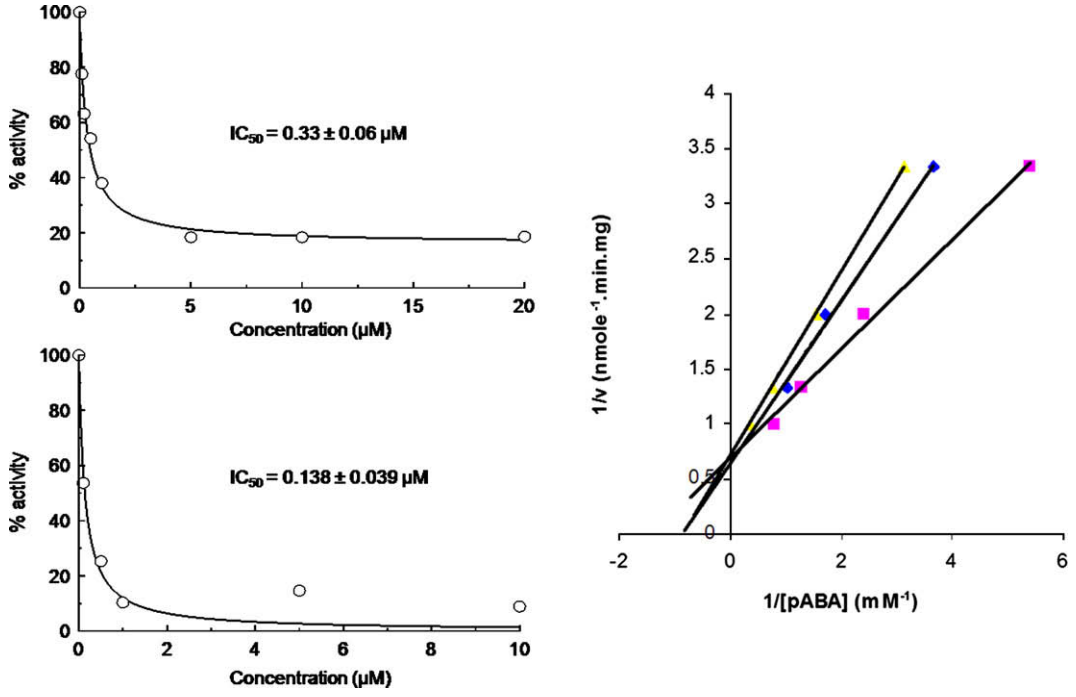

Figure 3. Dose–response curve for **5** versus purified recombinant human NAT1 (top left panel) and ZR-75 cell lysate (bottom left panel). IC_{50} values were calculated with Kyplot™ software. The assay of the recombinant enzyme was carried out using the hydrolysis of acetyl CoA assay in the presence of PABA as substrate (75 μM), whilst the assay with the ZR-75 cell lysate was carried out using the acetylation of arylamine assay in the presence of PABA as substrate (75 μM). (Right panel) Kinetic analysis of **5**: double reciprocal plot shows rates at inhibitor concentrations of 0 μM (square);0.05 μM (diamond) and 0.1 μM (triangle).

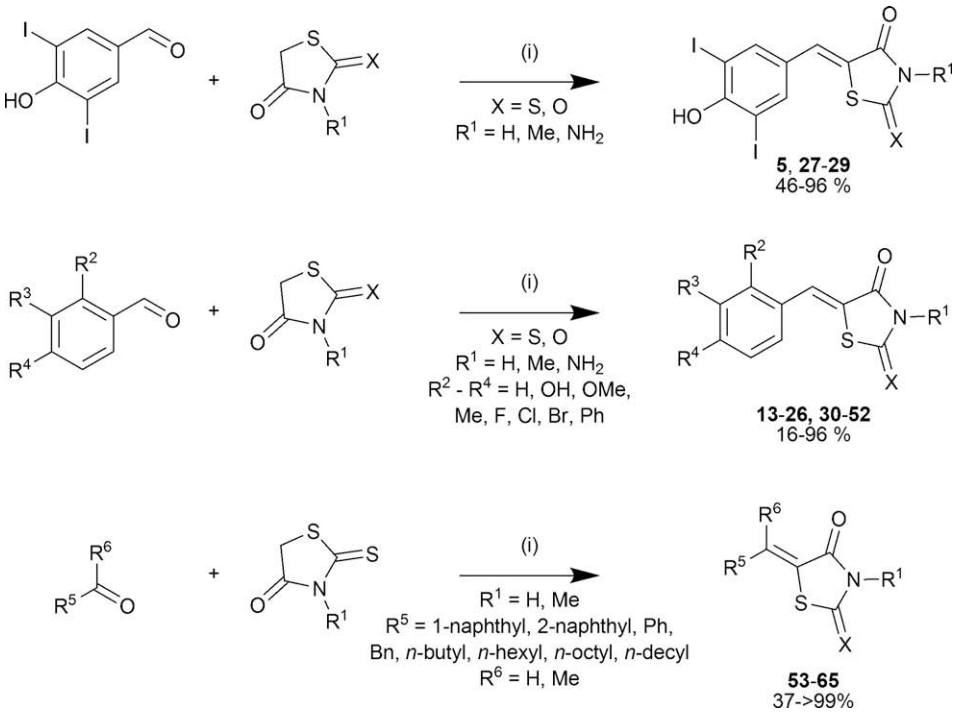

Scheme 2. Reagents and conditions: (i) NH_4OAc, toluene or ethyl acetate, reflux, 3–15 h.

Table 2
Varying the aryl substituent

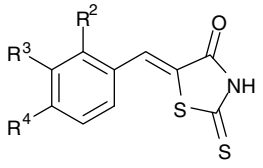

13-26

Compound	R^2	R^3	R^4	IC_{50} (μM)
13	H	H	OH	16.9
14	H	OH	H	0.6
15	OH	H	H	1.1
16	H	H	OMe	>30
17	H	OMe	H	>30
18	OMe	H	H	17.6
19	H	H	Me	>30
20	H	Me	H	17.0
21	Me	H	H	3.9
22	H	H	F	12.9
23	H	H	Cl	4.7
24	H	Cl	Cl	3.4
25	H	H	Ph	8.1
26	H	H	H	13.0

IC_{50} values determined versus human NAT1 using PABA substrate.

Table 3
Varying the heterocyclic core

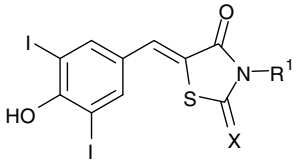

5, 27-29

Compound	X	R^1	IC_{50} (μM)
5	S	H	1.8
27	S	Me	7.6
28	S	NH_2	1.1
29	O	H	3.6

Structure–activity relationships were further probed in a combinatorial fashion, by varying both the aryl substitution and heterocyclic core simultaneously (Table 4). Consistent with earlier observations (Table 3), in most examples the inclusion of either an *N*-methyl or *N*-amino substituent was either observed to decrease NAT inhibitory activity compared to the parent compound or to have no significant effect. Interestingly, for the methoxy-substituted derivatives **34**–**36**, the inclusion of an *N*-methyl substituent was observed to reverse the trend observed in the corresponding *N*-unsubstituted series **16**–**18**: the most active *N*-unsubstituted derivative possessing an *ortho*-substituent (**18**, IC_{50} 17.6 μM) and the most active *N*-methyl derivative possessing a *para*-substituent (**34**, IC_{50} 1.0 μM). This may indicate a potential alternative binding mode for the *N*-methyl-substituted species.

Finally, the effect of incorporating fused aromatic or aliphatic groups on NAT inhibitory activity was assessed, along with the effect of including tetrasubstituted olefins (Table 5). The incorporation of a tetrasubstituted olefin moiety (**64** and **65**) was observed to diminish dramatically NAT inhibitory activity, as did the inclusion of a 1-naphthyl substituent (**56** and **57**). However, whilst a benzyl substituent (**58** and **59**) was not tolerated, those analogues containing a non-branched alkyl substituent (**60**–**63**) retained their activity. Moreover, a marked dependence of the inhibitory activity on alkyl chain length was observed, the optimal substituent being *n*-hexyl (**61**, IC_{50} 1.3 μM, Fig. 5).

2.5. Confirmation of binding mode of 5 within mouse Nat2

The full assignment of the ^1H NMR spectrum for mouse Nat2 has yet to be completed. However, ^1H–^{15}N HSQC experiments of ^{15}N-labelled mouse Nat2, and comparison of the spectra of mouse

Table 4
Varying both the aryl substituent and heterocyclic substituent

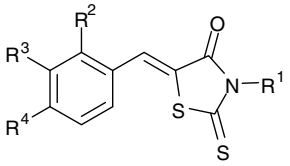

30-52

Compound	R^1	R^2	R^3	R^4	IC_{50} (μM)
30	Me	H	H	OH	14.0
31	NH_2	H	H	OH	10.1
32	Me	OH	H	H	20.1
33	NH_2	OH	H	H	5.1
34	Me	H	H	OMe	1.0
35	Me	H	OMe	H	13.6
36	Me	OMe	H	H	>30
37	Me	H	H	Me	>30
38	Me	H	Me	H	>30
39	Me	Me	H	H	4.4
40	Me	H	H	F	20.7
41	H	H	F	H	6.7
42	Me	H	F	H	7.3
43	H	F	H	H	>30
44	Me	F	H	H	11.8
45	Me	H	H	Cl	9.4
46	NH_2	H	H	Cl	5.7
47	H	H	H	Br	>30
48	Me	H	H	Ph	5.5
49	H	Ph	H	H	16.5
50	Me	Ph	H	H	10.1
51	NH_2	Ph	H	H	0.3
52	Me	H	H	H	>30

IC_{50} values determined versus mouse Nat2 using PABA as substrate.

Table 5
Varying both the aryl substituent and heterocyclic substituent

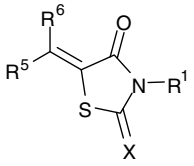

53-65

Compound	R^1	R^5	R^6	X	IC_{50} (μM)
53	H	2-Naphthyl	H	S	26.9
54	Me	2-Naphthyl	H	S	4.7
55	H	2-Naphthyl	H	O	>30
56	H	1-Naphthyl	H	S	>30
57	Me	1-Naphthyl	H	S	>30
58	H	Benzyl	H	S	24.2
59	Me	Benzyl	H	S	>30
60	H	*n*-Butyl	H	S	7.7
61	H	*n*-Hexyl	H	S	1.3
62	H	*n*-Octyl	H	S	6.8
63	H	*n*-Decyl	H	S	10.2
64	H	Ph	Me	S	25.0
65	Me	Ph	Me	S	>30

IC_{50} values determined versus mouse Nat2 using PABA as substrate.

Nat2 and other NAT isoforms led to the identification of four peaks in the 10- to 13-ppm region of the ^{1}H NMR spectrum; two of these peaks arise from the side-chain indole H^N of Trp67 and Trp132 and two from histidine side-chain imidazole H^N. NMR experiments with ^{15}N-labeled proteins showed that these four peaks are conserved between different NAT isoenzymes consistent with their location within the active site.[20]

The compounds studied here are only moderately soluble in aqueous solution and concentrated stock solutions for titrations must be prepared in DMSO. Separately, control studies have been performed to show that the protein tolerates up to 5% DMSO without loss of activity or significant shifts within the NMR spectrum. Upon addition of 0.2–1.0 equiv of **5** to the mouse Nat2 solution, the four characteristic peaks in the 10- to 13-ppm region decrease in intensity and a new set of peaks appear. Upon addition of 1.5 equiv of **5**, the four signals corresponding to unbound mouse Nat2 have disappeared completely, indicating saturation of the mouse Nat2-binding site with the compound (Fig. 6). This behaviour is characteristic of slow chemical exchange on the NMR timescale and is consistent with high-affinity binding of **5** to mouse Nat2. These observations are in contrast to the steroid derivatives previously reported as weak inhibitors of mouse Nat2 which showed gradual changes in chemical shift of these peaks with increasing inhibitor concentration, behaviour consistent with fast chemical exchange between bound and unbound states on the NMR timescale.[20] These observations are consistent with the higher inhibitory activity of **5** compared to the steroids, and could suggest either a relatively slow rate of exchange between bound and unbound states, or that the inhibitor is binding irreversibly (covalently) to the enzyme.

All of the four NMR signals in the 10- to 13-ppm region, previously assigned as being located within the active site of mouse Nat2, experience chemical shift perturbations upon inhibitor binding.[20] These data therefore support the kinetic studies, which revealed **5** to be a competitive inhibitor of mouse Nat2, and suggest that **5** binds directly to the active site.

2.6. In silico modelling

To probe the preferred binding mode of the NAT inhibitors identified to the protein, in silico docking studies were undertaken using the deposited crystal structure of human NAT1 (2PQT).[16] Simulated annealing was performed using AutoDock 4.[55] The docking solutions were very similar to results obtained using Gold (CCDC, v3.0.1)[56] and employing a homology model of human NAT1 previously generated from several existing structures of NAT isoforms.[17] The lowest energy conformations for the most potent inhibitors showed similar binding modes (Fig. 7 shows compound **15** as a representative example, docked into the crystal structure of human NAT1). The aryl substituent is predicted to extend into a hydrophobic pocket, with contact residues around the groove being Val^{93}, Phe^{125}, Val^{216} and Phe^{287}, providing a possible explanation for the preference for lipophilic substituents. Stabilisation also appears to be provided by two bonding interactions between Arg^{127} and both the carbonyl and 2′-hydroxy substituent of rhodanine **15**. Further stabilisation occurs through an additional hydrogen-bonding interaction between the 2′-hydroxy substituent of rhodanine **15** and the hydroxyl group of Thr^{289}. The additional hydrogen bonding may provide a partial explanation for the relatively high potency of 2′-hydroxyl-substituted rhodanine **15** over its 4′-hydroxyl-substituted rhodanine counterpart (**13**), for example. However, other factors must also be involved as non-hydrogen bonding substituents in the *ortho* position were also observed to give rise to enhanced potency over their *para*-substituted counterparts in some cases. Comparison of the binding mode of the inhibitors with human NAT1 compared to substrates such as 5AS, and the crystal structure of human NAT1 modified with bromoacetanilide,[16] reveals the inhibitor docking site to be partially overlapping with the 5AS and the α-substituted acetanilide moiety within the NAT1 crystal structure. The inhibitors would therefore be anticipated to block substrate binding, suggesting a competitive mode of inhibition of these compounds, consistent with the enzyme kinetic (Fig. 3) and the ^{1}H NMR studies (Fig. 6).

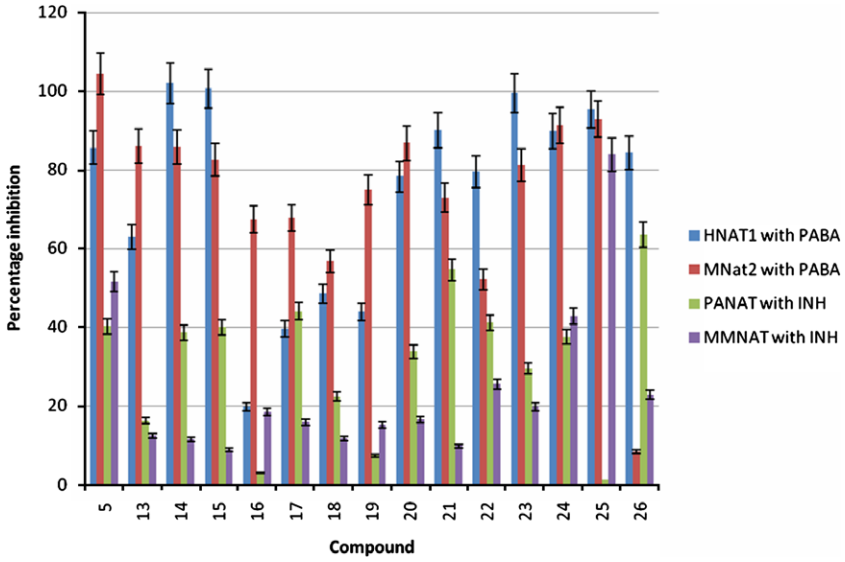

Figure 4. Structural analogues of **5**. Mean inhibition at 30 μM against MNat2 and HNAT1. MNat2 was screened using hydrolysis of AcCoA assay; HNAT1 was screened by acetylation of arylamine assay.

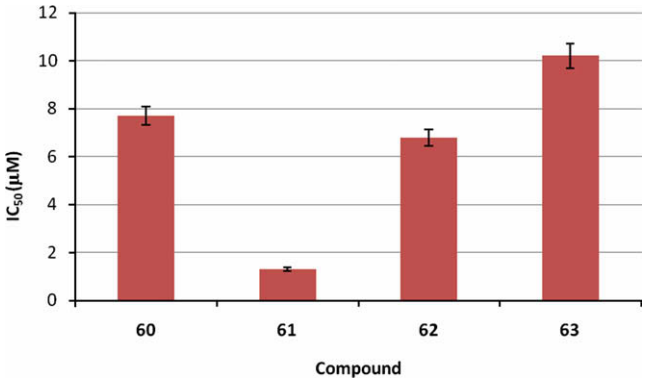

Figure 5. IC_{50} values determined for four alkyl-substituted rhodanines: **60** (R^5 = butyl); **61** (R^5 = hexyl); **62** (R^5 = octyl) and **63** (R^5 = decyl).

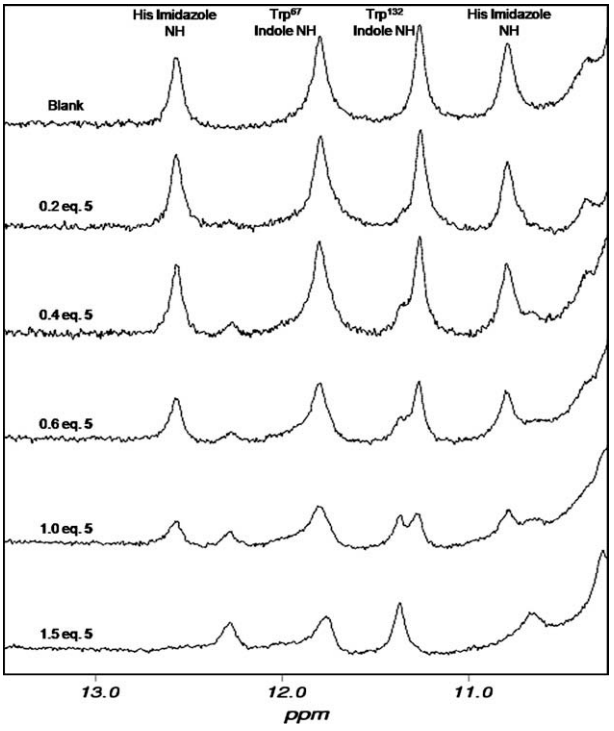

Figure 6. Partial ^1H NMR spectrum of varying equivalents of **5** bound to eq of mouse Nat2 protein; mouse Nat2 at 25.97 mg/mL (Section 3.2) was buffer exchanged into 10 mM Tris at pH 7.0 and 1 mM DTT;it was diluted to 12 mg/mL. Each sample contained mouse Nat2 (600 μL) and D2O (30 μL) with increasing concentrations of inhibitor. (600 MHz, 5% DMSO-d_6 in D_2O).

2.7. Cell-based toxicity studies

To be useable as a small-molecule tool to probe the role of human NAT1 or mouse Nat2 in a cellular context, the inhibitors needed to be non-toxic to cells. The most active inhibitors of mouse Nat2 **5**, **14**, **15**, **28**, **33** and **51** were therefore assessed for their effects on mouse macrophage (Table 6). With the exception of **5**, the original hit compound which showed >80% cell death relative to the control, none of the inhibitors showed significant toxicity at the same concentration. This preliminary data suggests that these inhibitors could become useful tools to dissect the role of the human NAT1 and mouse Nat2 enzymes in cells.

3. Conclusions

The identification, synthesis and evaluation of a series of rhodanine and thiazolidin-2,4-dione derivatives as selective inhibitors of human arylamine *N*-acetyltransferase 1 and mouse arylamine *N*-acetyltransferase 2 is described. The most potent inhibitors identified have submicromolar activity and inhibit both the recombinant proteins and human NAT1 in ZR-75 cell lysates in a competitive manner. ^1H NMR studies on purified mouse Nat2 demonstrate that the inhibitors bind within the putative active site of the enzyme. These tools will enable a clearer definition of the enzyme active site and may be used for further enzymological characterisation. Furthermore it is anticipated that they will enable investigations towards understanding the in vivo role of human NAT1 and mouse Nat2.

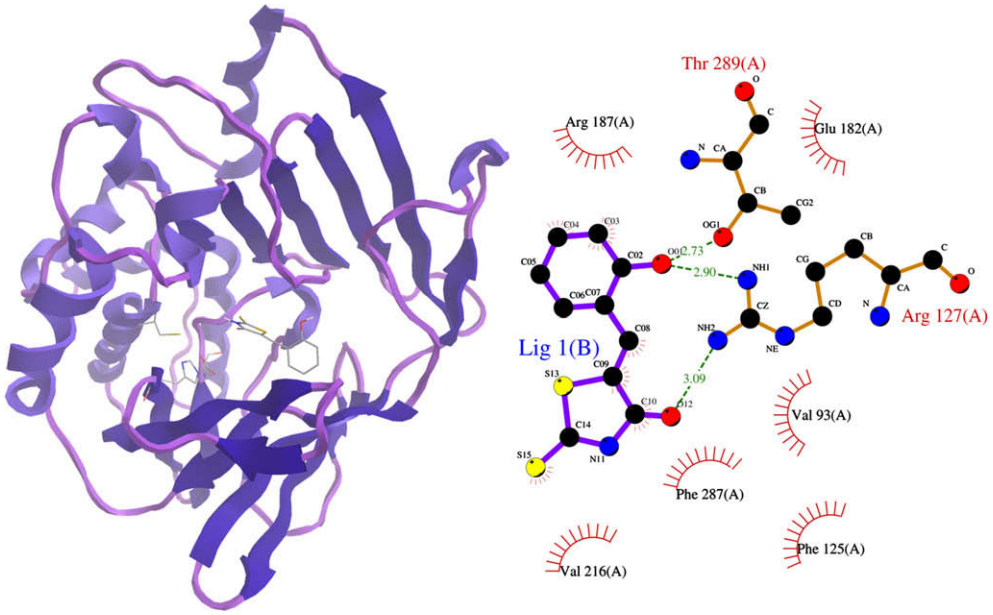

Figure 7. (Left) Binding of **15** with human NAT1: **15** is displayed in stick format;NAT1 is shown in ribbon format with the catalytic triad (Cys68, His107 and Asp122) displayed in stick format; (right) detail of active site region for **15** with human NAT1 showing two bonding interactions with Arg 127 and a hydrophobic pocket.

Table 6
Toxicity data for **5**, **16**, **17**, **30**, **35** and **54** at 10 μg/mL on mouse macrophage

	Toxicity[a]
DMSO	–
5	++
14	–
15	–
28	–
33	–
51	–

[a] ++, >80%; –, <80% cell death.

4. Experimental

4.1. Biology

4.1.1. Protein production

The recombinant NAT enzymes used in the primary screen were prepared as previously described, and are as follows: NATs from *P. aeruginosa* (PANAT),[15] *S. typhimurium* (STNAT),[48] and *M. smegmatis* (MSNAT),[14] NAT2 from Syrian hamsters,[17] and human NAT1.[17] The recombinant NAT enzymes used for the secondary screen were also prepared as previously described, and are as follows: NATs from *P. aeruginosa* (PANAT)[15] and *M. marinum* (MMNAT),[50] human NAT1, human NAT2, mouse Nat1 and mouse Nat2.[20]

The concentrations of solutions containing purified proteins were determined spectrophotometrically by measuring absorbances at 280 nm using calculated extinction coefficients (ε) for each enzyme. The purified NATs were stored in aliquots in 20 mM Tris–HCl (pH 8.0), 5 mM dithiothreitol, 5% glycerol, at −80 °C.

4.1.2. Enzymic assays

Two complementary assay methods were employed throughout: acetylation of arylamines or hydrolysis of AcCoA.

4.1.2.1. Acetylation of arylamines assay. The rates of arylamine acetylation by NATs were determined colorimetrically as previously described.[48] Each assay contained enzyme (in the cell lysate or recombinant enzyme as indicated), arylamine substrate (variable concentrations) and AcCoA (400 μM) in a total volume of 100 μL in assay buffer [20 mM Tris–HCl (pH 8.0), 1 mM DTT). Initially the enzyme and substrate mixtures were pre-incubated at 25 °C for 5 min and AcCoA was added to start the reaction. The reaction was quenched using 20% (w/v) trichloroacetic acid (TCA, 100 μL) at different time intervals. The stopped reaction was centrifuged (16,000*g*, 10 min) to pellet the precipitated proteins. The stopped reaction mixture (200 μL) was added to 5% (w/v) 4-(*N*,*N*-dimethylamino)benzaldehyde in 9:1 acetonitrile:water (800 μL) to develop the colour. The absorption at 450 nm was measured with a Hitachi U-2001 UV/vis spectrophotometer, with the amount of residual substrate in the reaction determined by comparison with a standard curve.

4.1.2.2. Hydrolysis of AcCoA. The rate of production of free thiol Coenzyme A by NATs in the presence of arylamine substrates and AcCoA was determined using Ellman's reagent, 5,5′-dithiobis(2-nitrobenzoic acid) [DTNB] as previously described.[11] The substrate (500 μM) and purified recombinant NAT were pre-incubated at 25 °C for 5 min in 96-well flat-bottomed polystyrene plates (Costar®, Corning Inc.) in 20 mM Tris–HCl (pH 8.0). AcCoA (400 μM) was added to start the reaction in a final volume of 100 μL. The reaction was quenched with the addition of 25 μL of guanidine–HCl solution [6.4 M guanidine–HCl, 0.1 M Tris–HCl, pH 7.3] containing 5 mM DTNB. The absorbance at 405 nm was measured on a plate-reader (Sunrise, Tecan). Assay buffer was used to replace substrate, AcCoA or NAT for control reactions. The amount of CoA produced in the assay was determined through comparison with a standard curve.

4.1.2.3. Primary screening assays. A previously described assay method determining the rate of hydrolysis of AcCoA[11] was adapted for use with a Beckman–Coulter Biomek 2000 liquid-handling robot, and used to identify inhibitors of the NAT-catalyzed acetylation of acetyl-acceptor substrates. To determine the appropriate assay time for each enzyme, preliminary manual assays were performed in which the assay time was varied, with a final concentration of acetylCoA of 400 μM and a final concentration of acetyl acceptor substrate of 500 μM. For each enzyme/substrate combination, an assay time was chosen which was both within the initial linear section on a graph of product concentration versus

time, and which gave absorbance readings between 0.3 and 0.8 absorbance units above time-zero measurements.

After the final addition of DTNB/guanidine stop reagent, the three replicate plates from each assay were transferred manually to the Tecan Sunrise plate reader, and the absorbances at 405 nm were measured. Once measured, the data were transferred to a custom spreadsheet (Microsoft Excel). The mean percentage inhibition and standard deviation across the replicate plates were automatically calculated, to highlight any anomalous data as early as possible, so that assays could be repeated if required. Data from each assay set were saved in separate files for subsequent data mining.

4.1.2.4. Data mining and hit-selection criteria. Raw data were mined by using custom-written scripts (Visual Basic) and saved in a single spreadsheet (Excel) for further analysis. Custom-written scripts were used to calculate the percentage inhibition, normal *Z*-score, improved *Z*-score and outlier and extreme outlier status for each data point as described elsewhere.[45] All custom-written scripts are available upon request.

4.1.2.5. Secondary assays. Following on from the primary screen of 5016 compounds, secondary assays were performed on the 223 hits from the initial screen. These 223 compounds comprised a subset of all of the compounds identified as hits (Table 2), and were chosen based on current projects in the authors' laboratory. Amongst the 223 compounds tested in the secondary screen were inhibitors specific for eukaryotic NATs, prokaryotic NATs and individual NAT enzymes (Table 2). The secondary assays were performed exactly as described for the primary assays, except for the pipetting sequence: the robot program was adjusted so that no multi-pipetting steps were present, to avoid systematic errors present in the primary screen (see below). The percentage inhibition scores in the secondary screen were used, as the median-based methods were not suitable, due to the high proportion of expected hits in the smaller secondary screen.

4.1.3. Protein NMR spectroscopy

ID ^{1}H NMR spectra for mouse Nat2 were collected at 20 °C using a jump-return sequence. This sequence enabled the observation of HN peaks arising from the imidazole side-chain of histidine which exchange to a significant extent with H_2O. Spectra were recorded using a sweep width of 12,500 Hz on a 600-MHz NMR spectrometer comprising an Oxford Instruments magnet, a triple-resonance gradient probe and a GE/Omega data acquisition system. Mouse Nat2 was used at a concentration of 10 mg/mL in the buffer described above, using 95% H_2O/10% D_2O. The titration of mouse Nat2 with compound 17 was performed by the stepwise addition of small volumes (5–20 μL) of a concentrated solution of 17 (10 mM in DMSO-d_6) to the mouse Nat2 solution in the NMR tube. The highest concentration of DMSO-d_6 in the sample used was 5%. DMSO alone had no effect on the NMR spectrum of mouse Nat2 at concentrations up to 5%.

4.1.4. Molecular modelling

For the homology model, the protein file was prepared in pdb format by using the AddH tool within the Chimera molecular modeling package.[57] The α-substituted acetanilide moiety was removed from Cys[68] of the deposited structure of human NAT1 (2PQT)[16] prior to docking being performed. Docking was performed with AutoDock 4[55] or Gold.[56] Ligand structures were drawn in ChemDraw (Cambridgesoft) and then converted to 3-dimensional structures in Chem3D. The molecules were energy-minimized with the MM2 force field and saved in sdf format for docking. The active site of the protein was defined by the Sγ atom of Cys[68] with an automatic cavity-detection radius of 20 Å. The docking solutions were ranked with the Autodock or Gold algorithms. Lowest-energy docking solutions were merged with the protein structure and saved in the pdb format, prior to visualisation with Chem3D (Cambridgesoft) or Aesop[13,58] as previously described.

4.1.5. Cell-based toxicity studies

Mouse macrophages were cultured in 25 cm^2 tissue culture bottles in RPMI/10% foetal calf serum in an atmosphere of 5% CO_2 at 37 °C. Cells were incubated in fresh medium for 24 h before addition of the inhibitor at a final concentration of 10 μg/mL by addition of 10 μL of stock solution in DMSO. A control containing DMSO only was used. The medium was removed after 72 h and the cells were detached from the container wall by adding 4 mL of LE (Lydocine EDTA). The solution of LE was centrifuged (900 rpm, 5 min) and the cell pellet was resuspended in fresh media by adding 100 μL to 100 μL of a 0.1% solution of Typan Blue. Live cells excluded Trypan Blue and dead cells are shown as a distinctive blue colour under a microscope. The numbers of dead cells were calculated microscopically using a haemocytometer. The dead cells were counted and compared with the positive control and at least 200 cells were counted in these separate estimates.

4.2. Chemistry

4.2.1. General experimental procedures

All reactions involving moisture-sensitive reagents were carried out under a nitrogen or argon atmosphere using standard vacuum line techniques and glassware that was flame-dried and cooled under nitrogen or argon before use. Solvents were dried according to the procedure outlined by Grubbs and co-workers.[59] Water was purified by an Elix® UV-10 system. All other solvents were used as supplied (analytical or HPLC grade) without prior purification. Organic layers were dried over $MgSO_4$ or Na_2SO_4 as stated. Thin layer chromatography was performed on aluminium plates coated with 60 F_{254} silica. Plates were visualised using UV light (254 nm), iodine, 1% aq $KMnO_4$ or 10% ethanolic phosphomolybdic acid. Column chromatography was performed on Kieselgel 60 silica. Elemental analyses were recorded by the microanalysis service of the Inorganic Chemistry Laboratory, University of Oxford, UK. Melting points were recorded on a Gallenkamp Hot Stage apparatus and are uncorrected. IR spectra were recorded on either a Perkin-Elmer Paragon 1000 FT-IR spectrometer or a Bruker Tensor 27 FT-IR spectrometer as either a thin film on NaCl plates (film) or a KBr disc (KBr), as stated. Selected characteristic peaks are reported in cm^{-1}. Nuclear magnetic resonance (NMR) spectra were recorded on Bruker DPX 400 (^{1}H: 400 MHz and ^{13}C: 100.6 MHz), AMX 500 (^{1}H: 500 MHz and ^{13}C: 125.3 MHz), Bruker DPX 250 (^{1}H: 250 MHz) or Varian 200 (^{1}H: 200 MHz) spectrometers in the deuterated solvent stated. All chemical shifts (δ) are quoted in ppm and coupling constants (J) in Hz. The field was locked by external referencing to the relevant deuteron resonance. Residual signals from the solvents were used as an internal reference. ^{13}C multiplicities were assigned using a DEPT sequence. Low-resolution mass spectra were recorded on either a VG MassLab 20-250 or a Micromass Platform 1 spectrometer. Accurate mass measurements were run on either a Bruker MicroTOF and were internally calibrated with polyalanine in positive and negative modes, or a Micromass GCT instrument fitted with a Scientific Glass Instruments BPX5 column (15 m × 0.25 mm) using amyl acetate as a lock mass.

4.2.2. Representative procedures

4.2.2.1. Representative procedure 1: formation of 2-thioxothiazolidine-4-one using toluene. The requisite carbonyl compound (1 equiv), 2-thioxothiazolidine-4-one **38** (1 equiv) and NH_4OAc (1 equiv) were refluxed in toluene for 12 h at 110 °C. The suspension was cooled and filtered, and the residual solid

was washed with hot MeOH to yield the crude product, which was purified by recrystallisation in DMSO/H_2O.

4.2.2.2. Representative procedure 2: formation of 2-thioxothiazolidine-4-one using ethyl acetate. The requisite carbonyl compound (1 equiv) heterocycle (1 equiv) in ethyl acetate with Et_3N (1 equiv) and AcOH (1 equiv) were refluxed at 85 °C for 3 h. The solution was cooled and heptane was added until a suspension formed, the suspension was then filtered and washed with heptane to yield the product, which was either purified by recrystallisation in DMSO/H_2O or column chromatography on silica.

4.2.3. (*Z*)-5-(3′,5′-Diiodo-4′-hydroxybenzylidene)-2-thioxothiazolidine-4-one (5)

3,5-Diiodo-4-hydroxybenzaldehyde (2.00 g, 5.3 mmol), 2-thioxothiazolidine-4-one (0.71 g, 5.3 mmol) and NH_4OAc (0.41 g, 5.3 mmol) in toluene (3 mL) were refluxed in the dark, under N_2 for 24 h. The suspension was cooled and filtered, and the residual solid was washed with hot MeOH to yield the crude product which was purified by recrystallisation with DMSO/H_2O to give **5** (2.45 g, 94%) as an orange solid; mp 282–284 °C (dec); {lit.[52] mp >285 °C}; ^{1}H NMR (400 MHz, DMSO-d_6): δ = 7.50 (1H, s, C=C*H*) and 7.94 (2H, s, Ar*H*).

4.2.4. (*Z*)-5-(4′-Hydroxybenzylidene)-2-thioxothiazolidin-4-one (13)

Following *representative procedure 1*: 4-hydroxybenzaldehyde (4.00 g, 32.0 mmol), 2-thioxothiazolidine-4-one (3.00 g, 22.5 mmol) and NH_4OAc (1.73 g, 22.5 mmol) in toluene (12 mL) gave **13** (2.45 g, 90%) as an orange solid; mp 279–280 °C (dec); {lit.[60] mp 287–290 °C}; ^{1}H NMR (400 MHz, DMSO-d_6): δ = 6.93 (2H, d, *J* = 8.7, Ar*H*), 7.47 (2H, d, *J* = 8.7, Ar*H*), 7.56 (1H, s, C=C*H*) and 10.44 (1H, br s, N*H*).

4.2.5. (*Z*)-5-(3′-Hydroxybenzylidene)-2-thioxothiazolidin-4-one (14)

Following *representative procedure 1*: 3-hydroxybenzaldehyde (0.237 g, 1.00 mmol), 2-thioxothiazolidin-4-one (0.133 g, 1.00 mmol) and NH_4OAc (0.077 g 1.00 mmol) in toluene (10 mL) gave **14** (0.192 g, 81%) as a brown solid; mp 237–239 °C; {lit.[61] mp 240–245 °C}; ^{1}H NMR (400 MHz, DMSO-d_6): δ = 6.87–6.91 (1H, m, Ar*H*), 6.97 (1H, m, Ar*H*), 7.05 (1H, d, *J* = 7.8, Ar*H*), 7.32–7.36 (1H, m, Ar*H*), 7.54 (1H, s, C=C*H*) and 9.86 (1H, s, N*H*).

4.2.6. (*Z*)-5-(2′-Hydroxybenzylidene)-2-thioxothiazolidin-4-one (15)

Following *representative procedure 1*: 2-hydroxybenzaldehyde (0.237 g, 1.00 mmol), 2-thioxothiazolidin-4-one (0.133 g, 1.00 mmol) and NH_4OAc (0.077 g, 1.00 mmol) in toluene (10 mL) gave **15** (0.038 g, 16%) as an orange solid; mp 224–225 °C; {lit.[53] mp 224–225 °C}; ^{1}H NMR (200 MHz, DMSO-d_6): δ = 6.90–7.04 (2H, m, Ar*H*), 7.31–7.42 (2H, m, Ar*H*), 7.86 (1H, s, C=C*H*) and 10.69 (1H, s, N*H*).

4.2.7. (*Z*)-5-(4′-Methoxybenzylidene)-2-thioxothiazolidin-4-one (16)

Following *representative procedure 1*: 4-methoxybenzaldehyde (0.251 g, 1.00 mmol), 2-thioxothiazolidin-4-one (0.133 g, 1.00 mmol) and NH_4OAc (0.077 g, 1.00 mmol) in toluene (10 mL) gave **16** (0.174 g, 69%) as an orange solid; mp 225–227 °C; {lit.[60] mp 233–235 °C}; ^{1}H NMR (400 MHz, DMSO-d_6): δ = 3.82 (3H, s, OCH_3), 7.09 (2H, d, *J* = 3.4, Ar*H*), 7.45 (1H, s, C=C*H*) and 7.53 (2H, d, *J* 3.4, Ar*H*).

4.2.8. (*Z*)-5-(3′-Methoxybenzylidene)-2-thioxothiazolidin-4-one (17)

Following *representative procedure 1*: 3-methoxybenzaldehyde (0.251 g, 1.00 mmol), 2-thioxothiazolidin-4-one (0.133 g, 1.00 mmol) and NH_4OAc (0.077 g, 1.00 mmol) in toluene (10 mL) gave **17** (0.196 g, 78%) as an orange solid; mp 224–225 °C; {lit.[61] mp 225–227 °C}; ^{1}H NMR (400 MHz, DMSO-d_6): δ = 3.81 (3H, s, OCH_3), 7.07 (1H, dd, *J* = 8.2, 1.7, Ar*H*), 7.15 (1H, s, Ar*H*), 7.16 (1H, dd, *J* = 8.2, 1.7, Ar*H*), 7.43–7.46 (1H, m, Ar*H*) and 7.59 (1H, s, C=C*H*).

4.2.9. (*Z*)-5-(2′-Methoxybenzylidene)-2-thioxothiazolidin-4-one (18)

Following *representative procedure 1*: 2-methoxybenzaldehyde (0.251 g, 1.00 mmol), 2-thioxothiazolidin-4-one (0.133 g, 1.00 mmol) and NH_4OAc (0.077 g, 1.00 mmol) in toluene (10 mL) gave **18** (0.174 g, 69%) as an orange solid; mp 205–206 °C; {lit.[62] mp 198–200 °C}; ^{1}H NMR (400 MHz, DMSO-d_6): δ = 3.90 (3H, s, OCH_3), 7.10 (1H, m, Ar*H*), 7.16 (1H, m, Ar*H*), 7.39 (1H, m, Ar*H*), 7.50 (1H, m, Ar*H*) and 7.79 (1H, s, C=C*H*).

4.2.10. (*Z*)-5-(4′-Methylbenzylidene)-2-thioxothiazolidin-4-one (19)

Following *representative procedure 1*: 4-methylbenzaldehyde (0.235 g, 1.00 mmol), 2-thioxothiazolidin-4-one (0.133 g, 1.00 mmol) and NH_4OAc (0.077 g, 1.00 mmol) in toluene (10 mL) gave **19** (0.156 g, 66%) as an orange solid; mp 219–220 °C {lit.[63] mp 219–220 °C}; ^{1}H NMR (400 MHz, DMSO-d_6): δ = 2.36 (3H, s, ArCH_3), 7.36 (2H, d, *J* = 8.2, Ar*H*), 7.50 (2H, d, *J* = 8.2, Ar*H*) and 7.61 (1H, s, C=C*H*).

4.2.11. (*Z*)-5-(3′-Methylbenzylidene)-2-thioxothiazolidin-4-one (20)

Following *representative procedure 1*: 2-methylbenzaldehyde (0.235 g, 1.00 mmol), 2-thioxothiazolidin-4-one (0.133 g, 1.00 mmol) and NH_4OAc (0.077 g, 1.00 mmol) in toluene (10 mL) gave **20** (0.178 g, 65%) as an orange solid; mp 180–181 °C; {lit.[63] mp 182–185 °C}; ^{1}H NMR (200 MHz, DMSO-d_6): δ = 2.38 (3H, s, ArCH_3), 7.34 (1H, s, Ar*H*), 7.39–7.57 (3H, m, Ar*H*) and 7.78 (1H, s, C=C*H*).

4.2.12. (*Z*)-5-(2′-Methylbenzylidene)-2-thioxothiazolidin-4-one (21)

Following *representative procedure 1*: 2-methylbenzaldehyde (0.235 g, 1.00 mmol), 2-thioxothiazolidin-4-one (0.133 g, 1.00 mmol) and NH_4OAc (0.077 g, 1.00 mmol) in toluene (10 mL) gave **21** (0.178 g, 75%) as an orange solid; mp 195–199 °C {lit.[63] mp 196 °C}; ^{1}H NMR (400 MHz, DMSO-d_6): δ = 2.42 (3H, s, ArCH_3), 7.10–7.54 (4H, m, Ar*H*) and 7.73 (1H, s, C=C*H*).

4.2.13. (*Z*)-5-(4′-Fluorobenzylidene)-2-thioxothiazolidin-4-one (22)

Following *representative procedure 1*: 4-fluorobenzaldehyde (0.251 g, 1.00 mmol), 2-thioxothiazolidin-4-one (0.133 g, 1.00 mmol) and NH_4OAc (0.077 g, 1.00 mmol) in toluene (10 mL) gave **22** (0.142 g, 59%) as an orange solid; mp 226–227 °C {lit.[63] mp 226–227 °C}; ^{1}H NMR (400 MHz, DMSO-d_6): δ = 7.32–7.44 (2H, m, Ar*H*) and 7.62–7.70 (3H, m, Ar*H* and C=C*H*).

4.2.14. (*Z*)-5-(4′-Chlorobenzylidene)-2-thioxothiazolidin-4-one (23)

Following *representative procedure 1*: 4-chlorobenzaldehyde (0.256 g, 1.00 mmol), 2-thioxothiazolidin-4-one (0.133 g, 1.00 mmol) and NH_4OAc (0.077 g, 1.00 mmol) in toluene (10 mL) gave **23** (0.172 g, 67%) as an orange solid; mp 228–229 °C; {lit.[60] mp 227–230 °C}; ^{1}H NMR (400 MHz, DMSO-d_6): δ = 7.56–7.68 (5H, m, Ar*H* and C=C*H*).

4.2.15. (*Z*)-5-(3′,4′-Dichlorobenzylidene)-2-thioxothiazolidin-4-one (24)

Following *representative procedure 1*: 3,4-dichlorobenzaldehyde (0.175 g, 1.00 mmol), 2-thioxothiazolidine-4-one (0.133 g, 1.00 mmol) and NH_4OAc (0.077 g, 1.00 mmol) in toluene (10 mL)

gave **24** (0.192 g, 67%) as a pure yellow solid; mp 231–233 °C; {lit.[63] mp 231–232 °C}; ^{1}H NMR (400 MHz, DMSO-d_6): δ = 7.53 (1H, d, J = 8.4, Ar*H*), 7.63 (1H, s, Ar*H*), 7.80 (1H, d, J = 8.4, Ar*H*) and 7.91 (1H, s, C=C*H*).

4.2.16. (*Z*)-5-(4′-Biphenylmethylene)-2-thioxothiazolidin-4-one (25)

Following *representative procedure 1*: 4-phenylbenzaldehyde (0.297 g, 1.00 mmol), 2-thioxothiazolidin-4-one (0.133 g, 1.00 mmol) and NH_4OAc (0.077 g, 1.00 mmol) in toluene (10 mL) gave **25** (0.138 g, 46%) as a red solid; mp 236–237 °C; {lit.[64] mp 239–240 °C}; ^{1}H NMR (400 MHz, DMSO-d_6): δ = 7.44 (2H, d, J = 7.6, Ar*H*), 7.51 (1H, m, Ar*H*), 7.69 (1H, s, C=C*H*), 7.71 (2H, m, Ar*H*), 7.76 (2H, d, J = 7.6, ArH) and 7.87 (2H, d, J = 8.4, Ar*H*).

4.2.17. (*Z*)-5-Benzylidene-2-thioxothiazolidin-4-one (26)

Following *representative procedure 1*: benzaldehyde (102 μL, 1.00 mmol), 2-thioxothiazolidin-4-one (0.133 g, 1.00 mmol) and NH_4OAc (0.077 g, 1.00 mmol), in toluene (10 mL) gave **26** (0.181 g, 82%) as a yellow solid; mp 203–205 °C; {lit.[60] mp 209–211 °C}; ^{1}H NMR (400 MHz, DMSO-d_6): δ = 7.47–7.84 (6H, m, Ar*H* and C=C*H*).

4.2.18. (*Z*)-5-(4′-Hydroxy-3′,5′-diiodobenzylidene)-3-methyl-2-thioxothiazolidin-4-one (27)

Following *representative procedure 2*: 4-hydroxy-3,5-diiodobenzaldehyde (0.373 g, 1.00 mmol) and 3-methyl-2-thioxothiazolidin-4-one (0.147 g, 1.00 mmol) gave **27** (0.2 g 40%) as an orange solid; mp 200–201 °C; IR (KBr): ν_{max}/cm^{-1} 3438 (O–H) 1700 (C=O) and 1597 (C=S); ^{1}H NMR (400 MHz, DMSO-d_6): δ = 3.39 (3H, s, NCH_3), 7.68 (1H, s, C=C*H*), 7.99 (2H, s, Ar*H*) and 9.92 (1H, br s, O*H*); ^{13}C NMR (100 MHz, DMSO-d_6): δ = 38.0, 85.7, 129.0, 129.2, 132.7, 139.6, 166.4, 168.4 and 193.9; LRMS (ESI$^-$): m/z 502 ([M−H]$^-$, 100%); HRMS (ESI$^-$): calcd for $C_{11}H_6I_2NO_2S_2$ [M−H]$^-$ 501.7929, found 501.7943.

4.2.19. (*Z*)-3-Amino-5-(4′-hydroxy-3′,5′-diiodobenzylidene)-2-thioxo-thiazolidin-4-one (28)

Following *representative procedure 2*: 4-hydroxy-3,5-diiodobenzaldehyde (0.373 g, 1.00 mmol) and 3-amino-2-thioxothiazolidin-4-one (0.148 g, 1.00 mmol) gave **28** (0.486 g, 96%) as an orange solid; mp 194–195 °C; IR (KBr): ν_{max}/cm^{-1} = 3438 (O–H), 1695 (C=O) and 1575 (C=S); ^{1}H NMR (400 MHz, DMSO-d_6): δ = 5.93 (2H, br s, NH_2), 7.67 (1H, s, C=C*H*), 7.97 (2H, s, Ar*H*) and 8.67 (1H, br s, O*H*); ^{13}C NMR (100 MHz, DMSO-d_6): δ = 87.3, 125.5, 128.6, 131.0, 141.8, 163.7, 169.4 and 193.1; LRMS (ESI$^-$): m/z 502 ([M−H]$^-$, 100%); HRMS (ESI$^-$): calcd for $C_{10}H_5I_2N_2O_2S_2$ [M−H]$^-$ 502.7882, found 502.7886.

4.2.20. (*Z*)-5-(4′-Hydroxy-3′,5′-diiodobenzylidene)thiazolidine-2,4-dione (29)

Following *representative procedure 2*: 4-hydroxy-3,5-diiodobenzaldehyde (0.373 g, 1.00 mmol) and thiazolidin-2,4-dione (0.116 g, 1.00 mmol) gave **29** (0.218 g, 46%) as an orange solid; mp 282–283 °C; {lit.[65] mp >285 °C); ^{1}H NMR (400 MHz, DMSO-d_6): δ = 7.69 (1H, s, C=C*H*), 7.98 (2H, s, Ar*H*) and 9.17 (1H, br s, N*H*).

4.2.21. (*Z*)-5-(4′-Hydroxybenzylidene)-3-methyl-2-thioxothiazolidin-4-one (30)

Following *representative procedure 2*: 4-hydroxybenzaldehyde (0.122 g, 1.00 mmol) and 3-methyl-2-thioxothiazolidin-4-one (0.147 g, 1.00 mmol) gave **30** (0.1 g 40%) as an orange solid; mp 194–195 °C; ^{1}H NMR (400 MHz, DMSO-d_6): δ = 3.38 (3H, s, NCH_3), 6.93 (2H, d, J = 8.7, Ar*H*), 7.47 (2H, d, J = 8.7, Ar*H*), 7.56 (1H, s, C=C*H*) and 9.67 (1H, br s, O*H*).

4.2.22. (*Z*)-3-Amino-5-(4′-hydroxybenzylidene)-2-thioxothiazolidin-4-one (31)

Following *representative procedure 2*: 4-hydroxybenzaldehyde (0.122 g, 1.00 mmol) and 3-amino-2-thioxothiazolidin-4-one (0.148 g, 1.00 mmol), gave **31** (0.19 g; 75%) as an orange solid; mp 190–191 °C; IR (KBr): ν_{max}/cm^{-1} = 3404 (O—H), 1703 (C=O) and 1582 (C=S); ^{1}H NMR (400 MHz, DMSO-d_6): δ = 5.94 (2H, s, NH_2), 6.92 (2H, d, J = 7.7, Ar*H*), 7.11 (2H, d, J = 7.7, Ar*H*), 7.76 (1H, s, C=C*H*), 9.91 (1H, br s, O*H*); ^{13}C NMR (50 MHz, DMSO-d_6): δ = 115.3–158.0 (8 × C), 167.6 and 194.4; LRMS (ESI$^-$): m/z 251 ([M−H]$^-$, 100%); HRMS (ESI$^-$): calcd for $C_{10}H_7N_2O_2S_2$ [M−H]$^-$ 250.9949, found 250.9943.

4.2.23. (*Z*)-5-(2′-Hydroxybenzylidene)-3-methyl-2-thioxothiazolidin-4-one (32)

Following *representative procedure 2*: 2-hydroxybenzaldehyde (0. 122 g, 1.00 mmol) and 3-methyl-2-thioxothiazolidin-4-one (0.147 g, 1.00 mmol) gave **32** (0.158 g, 63%) as an orange solid; mp 144–145 °C; ^{1}H NMR (200 MHz, DMSO-d_6): δ = 3.32 (3H, s, NCH_3), 6.91–7.03 (2H, m, Ar*H*), 7.30–7.42 (2H, m, Ar*H*), 8.01 (1H, s, C=C*H*) and 10.76 (1H, br s, O*H*).

4.2.24. (*Z*)-3-Amino-5-(2′-hydroxybenzylidene)-2-thioxothiazolidin-4-one (33)

Following *representative procedure 2*: 2-hydroxybenzaldehyde (0.122 g, 1.00 mmol) and 3-amino-2-thioxothiazolidin-4-one (0.148 g, 1.00 mmol) gave **33** (0.194 g, 77%) as an orange solid; mp 198–200 °C; ^{1}H NMR (400 MHz, DMSO-d_6): δ = 5.94 (2 H, s, NH_2), 6.92–7.36 (4H, m, Ar*H*), 7.78 (1H, s, C=C*H*) and 10.11 (1H, br s, O*H*).

4.2.25. (*Z*)-5-(4′-Methoxybenzylidene)-3-methyl-2-thioxothiazolidin-4-one (34)

Following *representative procedure 2*: 4-methoxybenzaldehyde (0.136 g, 1.00 mmol) and 3-methyl-2-thioxothiazolidin-4-one (0.147 g, 1.00 mmol) gave **34** (0.214 g, 81%) as an orange solid; mp 175–176 °C; {lit.[66] mp 181 °C}; δ_H (400 MHz, DMSO-d_6) 3.39 (3H, s, NCH_3), 3.82 (3H, s, OCH_3), 7.09 (2H, d, J = 3.4, Ar*H*), 7.45 (1H, s, C=C*H*) and 7.53 (2H, d, J = 3.4, Ar*H*).

4.2.26. (*Z*)-5-(3′-Methoxybenzylidene)-3-methyl-2-thioxothiazolidin-4-one (35)

Following *representative procedure 2*: 3-methoxybenzaldehyde (0.136 g, 1.00 mmol) and 3-methyl-2-thioxothiazolidin-4-one (0.147 g, 1.00 mmol) gave **35** (0.210 g, 79%) as an orange solid; mp 139–141 °C; {lit.[67] mp 140–142 °C}; ^{1}H NMR (200 MHz, DMSO-d_6): δ = 3.40 (3H, s, NCH_3), 3.82 (3H, s, OCH_3), 7.10 (1H, dd, J = 7.8, 2.0, Ar*H*), 7.15–7.26 (2H, m, Ar*H*), 7.48 (1H, s, Ar*H*) and 7.80 (1H, s, C=C*H*).

4.2.27. (*Z*)-5-(2′-Methoxybenzylidene)-3-methyl-2-thioxothiazolidin-4-one (36)

Following *representative procedure 2*: 2-methoxybenzaldehyde (0.136 g, 1.00 mmol) and 3-methyl-2-thioxothiazolidin-4-one (0.147 g, 1.00 mmol), gave **36** (0.224 g, 85%) as an orange solid; mp 180–181 °C; {lit.[67] mp 188–190 °C}; ^{1}H NMR (200 MHz, DMSO-d_6): δ = 3.40 (3H, s, NCH_3), 3.92 (3H, s, OCH_3), 6.99–7.61 (4H, m, Ar*H*) and 7.95 (1H, s, C=C*H*).

4.2.28. (*Z*)-3-Methyl-5-(4′-methylbenzylidene)-2-thioxothiazolidin-4-one (37)

Following *representative procedure 2*: 4-methylbenzaldehyde (0.120 g, 1.00 mmol) and 3-methyl-2-thioxothiazolidin-4-one (0.147 g, 1.00 mmol) gave **37** (0.164 g, 66%) as an orange solid; mp 168–169 °C; {lit.[63] mp 169.5–170 °C}; ^{1}H NMR (400 MHz, DMSO-d_6): δ = 2.37 (3H, s, ArCH_3), 3.42 (3H, s, NCH_3), 7.38

(2H, d, J = 6.8, Ar*H*), 7.55 (2H, d, J = 6.8, Ar*H*) and 7.79 (1H, s, C=C*H*).

4.2.29. (*Z*)-3-Methyl-5-(3′-methylbenzylidene)-2-thioxothiazolidin-4-one (38)

Following *representative procedure 2*: 3-methylbenzaldehyde (0.120 g, 1.00 mmol) and 3-methyl-2-thioxothiazolidin-4-one (0.147 g, 1.00 mmol), gave **38** (0.183 g, 74%) as an orange solid; mp 162–164 °C; {lit.[63] mp 164–167 °C}; ^{1}H NMR (200 MHz, DMSO-d_6): δ = 2.38 (3H, s, ArCH_3), 3.42 (3H, s, NCH_3), 7.34 (1H, s, Ar*H*), 7.39–7.57 (3H, m, Ar*H*) and 7.78 (1H, s, C=C*H*).

4.2.30. (*Z*)-3-Methyl-5-(2′-methylbenzylidene)-2-thioxothiazolidin-4-one (39)

Following *representative procedure 2*: 2-methylbenzaldehyde (0.120 g, 1.00 mmol) and 3-methyl-2-thioxothiazolidin-4-one (0.147 g, 1.00 mmol) gave **39** (0.196 g, 79%) as an orange solid; mp 148–149 °C; IR (KBr): ν_{max}/cm^{-1} 1715 (C=O) and 1604 (C=S); ^{1}H NMR (500 MHz, DMSO-d_6): δ = 2.43 (3H, s, ArCH_3), 3.41 (3H, s, NCH_3), 7.33–7.47 (4H, m, Ar*H*) and 7.91 (1H, s, C=C*H*); ^{13}C NMR (126 MHz, DMSO-d_6): δ = 19.5, 31.3, 123.4–133.2 (7 × C), 139.3, 166.8 and 194.2; LRMS (ESI$^-$): m/z 248 ([M−H]$^-$, 100%); HRMS (ESI$^-$): calcd for $C_{12}H_{11}NNaOS_2$ [M+Na]$^+$ 272.0180, found 272.0174.

4.2.31. (*Z*)-5-(4′-Fluorobenzylidene)-3-methyl-2-thioxothiazolidin-4-one (40)

Following *representative procedure 2*: 4-fluorobenzaldehyde (0.124 g, 1.00 mmol) and 3-methyl-2-thioxothiazolidin-4-one (0.147 g, 1.00 mmol) gave **40** (0.162 g, 64%) as an orange solid; mp 184–185 °C; IR (KBr): ν_{max}/cm^{-1} = 1711 (C=O) and 1593 (C=S); ^{1}H NMR (400 MHz, DMSO-d_6): δ = 3.33 (3H, s, NCH_3), 7.26–7.54 (2H, m, Ar*H*), 7.64–7.81 (2H, m, Ar*H*) and 7.84 (1H, s, C=C*H*); ^{13}C NMR (50 MHz, DMSO-d_6): δ = 31.6, 117.3, 132.0, 133.5, 133.7, 139.2, 166.2, 166.8 and 192.9; LRMS (ESI$^+$): m/z 253 ([M+H]$^+$, 100%); HRMS (ESI$^+$): calcd for $C_{11}H_9FNOS_2$ [M+H]$^+$ 254.0110, found 254.0103.

4.2.32. (*Z*)-5-(3′-Fluorobenzylidene)-2-thioxothiazolidin-4-one (41)

Following *representative procedure 2*: 3-fluorobenzaldehyde (0.124 g, 1.00 mmol) and 2-thioxothiazolidin-4-one (0.133 g, 1.00 mmol) gave **41** (0.124 g, 52%) as an orange solid; mp 201–202 °C; {lit.[63] mp 201 °C}; ^{1}H NMR (400 MHz, DMSO-d_6): δ = 7.39–7.59 (4H, m, Ar*H*) and 7.83 (1H, s, C=C*H*).

4.2.33. (*Z*)-5-(3′-Fluorobenzylidene)-3-methyl-2-thioxothiazolidin-4-one (42)

Following *representative procedure 2*: 3-fluorobenzaldehyde (0.124 g, 1.00 mmol) and 3-methyl-2-thioxothiazolidin-4-one (0.147 g, 1.00 mmol) gave **42** (0.176 g, 70%) as an orange solid; mp 163–164 °C; IR (KBr): ν_{max}/cm^{-1} = 1710 (C=O) and 1602 (C=S); ^{1}H NMR (400 MHz, DMSO-d_6): δ = 3.42 (3H, s, NCH_3), 7.35–7.65 (4H, m, Ar*H*) and 7.83 (1H, s, C=C*H*); ^{13}C NMR (50 MHz, DMSO-d_6): δ = 32.6, 118.3, 133.6–133.8 (5 × C), 139.5, 169.1, 165.8 and 196.9; LRMS (FI$^+$): m/z 253 ([M]$^+$, 100%); HRMS (FI$^+$): calcd for $C_{11}H_8FNOS_2$ [M]$^+$ 253.0031, found 253.0036.

4.2.34. (*Z*)-5-(2′-Fluorobenzylidene)-2-thioxothiazolidin-4-one (43)

Following *representative procedure 2*: 2-fluorobenzaldehyde (0.124 g, 1.00 mmol) and 2-thioxothiazolidin-4-one (0.133 g, 1.00 mmol) gave **43** (0.113 g, 47%) as an orange solid; mp 201–203 °C; {lit.[63] mp 201–203 °C}; ^{1}H NMR (400 MHz, DMSO-d_6): δ = 7.31–7.40 (2H, m, Ar*H*), 7.48 (1H, s, C=C*H*) and 7.49–7.56 (2H, m, Ar*H*).

4.2.35. (*Z*)-5-(2′-Fluorobenzylidene)-3-methyl-2-thioxothiazolidin-4-one (44)

Following *representative procedure 2*: 2-fluorobenzaldehyde (0.124 g, 1.00 mmol) and 3-methyl-2-thioxothiazolidin-4-one (0.147 g, 1.00 mmol) gave **44** (0.207 g, 82%) as an orange solid; mp 171–173 °C; $C_{11}H_8FNOS_2$ requires C 52.2, H 3.2, N 5.5%, found: C 52.0, H 3.1, N 5.6%; IR (KBr): ν_{max}/cm^{-1} = 1709 (C=O) and 1603 (C=S); ^{1}H NMR (400 MHz, DMSO-d_6): δ = 3.56 (3H, s, NCH_3), 7.44–7.64 (2H, m, Ar*H*), 7.65–7.82 (2H, m, Ar*H*) and 7.93 (1H, s, C=C*H*); ^{13}C NMR (125 MHz, DMSO-d_6): δ = 31.3, 116.3, 120.8, 123.5, 125.4, 125.7, 129.6, 133.3, 133.4, 166.9 and 193.5; LRMS (FI$^+$): m/z 253 ([M]$^+$, 100%); HRMS (FI$^+$): calcd for $C_{11}H_8FNOS_2$ [M]$^+$ 253.0031, found 253.0037.

4.2.36. (*Z*)-5-(4′-Chlorobenzylidene)-3-methyl-2-thioxothiazolidin-4-one (45)

Following *representative procedure 2*: 4-chlorobenzaldehyde (0.140 g, 1.00 mmol) and 3-methyl-2-thioxothiazolidin-4-one (0.147 g, 1.00 mmol) gave **45** (0.259 g, 96%) as an orange solid; mp 192–195 °C; {lit.[63] mp 198–200 °C}; ^{1}H NMR (200 MHz, DMSO-d_6): δ = 3.40 (3H, s, NCH_3), 7.09–7.81 (4H, m, Ar*H*) and 7.83 (1H, s, C=C*H*).

4.2.37. (*Z*)-3-Amino-5-(4′-chlorobenzylidene)-2-thioxothiazolidin-4-one (46)

Following *representative procedure 2*: 4-chlorobenzaldehyde (0.140 g, 1.00 mmol) and 3-amino-2-thioxothiazolidin-4-one (0.148 g, 1.00 mmol) gave **46** (0.208 g, 82%) as an orange solid; mp 210–211 °C; ^{1}H NMR (400 MHz, DMSO-d_6): δ = 5.94 (2H, br s, NH_2), 7.21–7.78 (4H, m, Ar*H*) and 7.85 (1H, s, C=C*H*).[67]

4.2.38. (*Z*)-5-(4′-Bromobenzylidene)-2-thioxothiazolidin-4-one (47)

Following *representative procedure 2*: 4-bromobenzaldehyde (0.184 g, 1.00 mmol) and 2-thioxothiazolidin-4-one (0.133 g, 1.00 mmol) gave **47** (0.195 g, 65%) as an orange solid; mp 238–239 °C; {lit.[68] mp 231 °C}; ^{1}H NMR (200 MHz, DMSO-d_6): δ = 7.59 (2H, d, J = 5.2, Ar*H*), 7.75 (1H, s, C=C*H*) and 7.81 (2H, d, J = 5.2, Ar*H*).

4.2.39. (*Z*)-5-(4′-Biphenylmethylene)-3-methyl-2-thioxothiazolidin-4-one (48)

Following *representative procedure 2*: 4-phenylbenzaldehyde (0.182 g, 1.00 mmol) and 3-methyl-2-thioxothiazolidin-4-one (0.147 g, 1.00 mmol) gave **48** (0.208 g, 67%) as an orange solid; mp 144–145 °C; IR (KBr): ν_{max}/cm^{-1} = 1711 (C=O) and 1591 (C=S); ^{1}H NMR (200 MHz, DMSO-d_6): δ = 3.37 (3H, s, NCH_3), 7.17–7.70 (10H, m, Ar*H* and C=C*H*); ^{13}C NMR (126 MHz, DMSO-d_6): δ = 30.8, 121.3–133.4 (12 × C), 138.6, 142.2, 167.0 and 193.4; LRMS (FI$^+$): m/z 311 ([M]$^+$, 100%); HRMS (FI$^+$): calcd for $C_{17}H_{13}NOS_2$ [M]$^+$ 311.0439, found 311.0432.

4.2.40. (*Z*)-5-(Biphenyl-2′-ylmethylene)-2-thioxothiazolidin-4-one (49)

Following *representative procedure 2*: 2-phenylbenzaldehyde (0.182 g, 1.00 mmol) and 2-thioxothiazolidin-4-one (0.133 g, 1.00 mmol) gave **49** (0.152 g, 51%) as an orange solid; mp 242–243 °C; {lit.[69] mp 243–244 °C}; ^{1}H NMR (200 MHz, DMSO-d_6): δ = 6.86–8.06 (10H, m, Ar*H* and C=C*H*).

4.2.41. (*Z*)-5-(Biphenyl-2′-ylmethylene)-3-methyl-2-thioxothiazolidin-4-one (50)

Following *representative procedure 2*: 2-phenylbenzaldehyde (0.182 g, 1.00 mmol) and 3-methyl-2-thioxothiazolidin-4-one (0.147 g, 1.00 mmol) gave **50** (0.243 g, 78%) as an orange solid; mp 150–151 °C; IR (KBr): ν_{max}/cm^{-1} = 1709 (C=O) and 1585 (C=S); ^{1}H NMR (400 MHz, DMSO-d_6): δ = 3.37 (3H, s, NCH_3),

7.26–7.40 (2H, m, Ar*H*), 7.43–7.55 (5H, m, Ar*H*), 7.57–7.95 (3H, m, Ar*H* and C=C*H*); ^{13}C NMR (100 MHz, DMSO-d_6): δ = 30.9, 120.2–135.0 (12 × C), 139.3, 143.4, 172.5 and 191.7; LRMS (FI$^+$): *m/z* 311 ([M]$^+$, 100%); HRMS (FI$^+$): calcd for $C_{17}H_{13}NOS_2$ [M]$^+$ 311.0439, found 311.0436.

4.2.42. (*Z*)-3-Amino-5-(biphenyl-2′-ylmethylene)-2-thioxothiazolidin-4-one (51)

Following *representative procedure 2*: 2-phenylbenzaldehyde (0.182 g, 1.00 mmol) and 3-amino-2-thioxothiazolidin-4-one (0.148 g, 1.00 mmol) gave **51** (0.213 g, 68%) as an orange solid; mp 168–169 °C; ^{1}H NMR (400 MHz, DMSO-d_6): δ = 5.36 (2H, s NH_2), 7.26–7.40 (2H, m, Ar*H*), 7.43–7.55 (5H, m, Ar*H*) and 7.55–7.68 (3H, m, Ar*H* and C=C*H*).

4.2.43. (*Z*)-5-Benzylidene-3-methyl-2-thioxothiazolidin-4-one (52)

Following *representative procedure 2*: benzaldehyde (0.106 g, 1.00 mmol) and 3-methyl-2-thioxothiazolidin-4-one (0.147 g, 1.00 mmol) gave **52** (0.219 g, 93%) as an orange solid; mp 170–172 °C; {lit.[70] mp 179–181 °C}; ^{1}H NMR (400 MHz, DMSO-d_6): δ = 3.41 (3H, s, NCH_3), 7.41–7.61 (3 H, m, Ar*H*), 7.66 (2H, d, *J* = 7.3, Ar*H*) and 7.84 (1H, s, C=C*H*).

4.2.44. (*Z*)-5-(Naphthalen-2′-ylmethylene)-2-thioxothiazolidin-4-one (53)

Following *representative procedure 2*: 2-naphthaldehyde (0.156 g, 1.00 mmol) and 2-thioxothiazolidin-4-one (0.133 g, 1.00 mmol) gave **53** (0.134 g, 50%) as an orange solid; mp 269–270 °C; {lit.[71] mp 269–270 °C}; ^{1}H NMR (400 MHz, DMSO-d_6): δ = 7.42–8.31 (8H, m, Ar*H* and C=C*H*).

4.2.45. (*Z*)-3-Methyl-5-(naphthalen-2′-ylmethylene)-2-thioxothiazolidin-4-one (54)

Following *representative procedure 2*: 2-naphthaldehyde (0.156 g, 1.00 mmol) and 3-methyl-2-thioxothiazolidin-4-one (0.147 g, 1.00 mmol) gave **54** (0.104 g, 37%) as an orange solid; mp 242–244 °C; {lit.[72] mp 242–243 °C}; ^{1}H NMR (400 MHz, DMSO-d_6): δ = 3.44 (3H, s, NCH_3) and 7.57–8.29 (8H, m, Ar*H* and C=C*H*).

4.2.46. (*Z*)-5-(Naphthalen-2′-ylmethylene)thiazolidine-2,4-dione (55)

Following *representative procedure 2*: 2-naphthaldehyde (0.156 g, 1.00 mmol) and thiazolidin-2,4-dione (0.117 g, 1.00 mmol) gave **55** (0.134 g, 53%) as an orange solid; mp 250–251 °C; ^{1}H NMR (400 MHz, DMSO-d_6): δ = 7.62 (1H, m, Ar*H*), 7.70 (1H, d, *J* = 8.7, Ar*H*), 7.95 (1H, s, C=C*H*), 7.98 (1H, d, *J* = 7.6, Ar*H*), 8.02–8.09 (3H, m, Ar*H*) and 8.20 (1H, s, Ar*H*).

4.2.47. (*Z*)-5-(Naphthalen-1′-ylmethylene)-2-thioxothiazolidin-4-one (56)

Following *representative procedure 2*: 1-naphthaldehyde (0.156 g, 1.00 mmol) and 2-thioxothiazolidin-4-one (0.133 g, 1.00 mmol) gave **56** as an orange solid (0.270 g, 100%); mp 229–232 °C; {lit.[71] mp 224–225 °C}; ^{1}H NMR (400 MHz, DMSO-d_6): δ = 7.37–8.44 (8H, m, Ar*H* and C=C*H*) and 10.41 (1H, s, N*H*).

4.2.48. (*Z*)-3-Methyl-5-(naphthalen-1′-ylmethylene)-2-thioxothiazolidin-4-one (57)

Following *representative procedure 2*: 1-naphthaldehyde (0.156 g, 1.00 mmol) and 3-methyl-2-thioxothiazolidin-4-one (0.147 g, 1.00 mmol) gave **57** (0.116 g, 41%) as an orange solid; mp 146–148 °C; {lit.[72] mp 141–142 °C}; ^{1}H NMR (400 MHz, DMSO-d_6): δ = 3.65 (3H, s, NCH_3), 7.17–8.54 (8H, m, Ar*H* and C=C*H*) and 9.95 (1H, s, N*H*).

4.2.49. (*Z*)-5-(2′-Phenylethylidene)-2-thioxothiazolidin-4-one (58)

Following *representative procedure 2*: phenylacetaldehyde (0.146 g, 1.00 mmol) and 2-thioxothiazolidin-4-one (0.133 g, 1.00 mmol) gave **58** (0.176 g, 75%) as an orange solid; mp 293–294 °C; IR (KBr): ν_{max}/cm^{-1} = 1698 (C=O) and 1579 (C=S); ^{1}H NMR (400 MHz, DMSO-d_6): δ =3.35 (2H, m, CH_2Ar), 6.15 (1H, m, C=C*H*), 7.06–7.23 (3H, m, Ar*H*) and 7.58 (2H, d, *J* = 8.6, Ar*H*); ^{13}C NMR (100 MHz, DMSO-d_6): δ = 30.3, 113.0–162.6 (8 × C), 167.9 and 192.2; LRMS (FI$^+$): *m/z* 235 ([M]$^+$, 100%); HRMS (FI$^+$): calcd for $C_{11}H_9NOS_2$ [*M*]$^+$ 235.0126, found 235.0129.

4.2.50. (*Z*)-3-Methyl-5-(2′-phenylethylidene)-2-thioxothiazolidin-4-one (59)

Following *representative procedure 2*: phenylacetaldehyde (0.146 g, 1.00 mmol) and 3-methyl-2-thioxothiazolidin-4-one (0.147 g, 1.00 mmol) gave **59** (0.265 g, 95%) as an orange solid; mp 208–209 °C; IR (KBr): ν_{max}/cm^{-1} = 1702 (C=O) and 1587 (C=S); ^{1}H NMR (500 MHz, DMSO-d_6): δ = 3.38 (3H, s, NCH_3), 3.48–3.53 (2H, m, CH_2Ar), 7.23–7.78 (6H, m, Ar*H* and C=C*H*); ^{13}C NMR (125 MHz, DMSO-d_6): δ = 29.0, 31.3, 111.5–163.2 (6 × C), 166.9 and 193.4; LRMS (ESI$^+$): 272 ([M+Na]$^+$, 100%); HRMS (ESI$^+$): calcd for $C_{12}H_{11}NNaOS_2$ [M+Na]$^+$ 272.0180, found 272.0168.

4.2.51. (*Z*)-5-Butylidene-2-thioxothiazolidin-4-one (60)

Following *representative procedure 2*: *n*-butyraldehyde (90 μL, 1.00 mmol) was distilled and added to 2-thioxothiazolidin-4-one (0.133 g, 1.00 mmol) gave **60** (0.026 g, 15%) as a yellow oil after aqueous work up; ^{1}H NMR (400 MHz, DMSO-d_6): δ = 0.97–0.99 (3H, m, CH_3), 1.53–1.55 (2H, m, CH_2CH$_3$), 2.56–2.58 (2H, m, C=C*H*CH_2) and 6.29–6.31 (1H, m, C=C*H*).

4.2.52. (*Z*)-5-Hexylidene-2-thioxothiazolidin-4-one (61)

Following *representative procedure 2*: *n*-hexanal (122 μL, 1.00 mmol) was distilled and added to 2-thioxothiazolidin-4-one (0.133 g, 1.00 mmol) gave **61** (0.04 g, 19%) as a yellow oil; ^{1}H NMR (400 MHz, DMSO-d_6): δ = 0.97–0.99 (3H, m, CH_3), 1.24–1.74 (6H, m, —CH_2—), 2.65–2.68 (2H, m, C=C*H*CH_2) and 6.31–6.33 (1H, m, C=C*H*).

4.2.53. (*Z*)-5-Octylidene-2-thioxothiazolidin-4-one (62)

Following *representative procedure 2*: *n*-octanal (156 μL, 1.00 mmol) was distilled and added to 2-thioxothiazolidin-4-one (0.133 g, 1.00 mmol) gave **62** (0.0267 g, 11%) as a yellow oil; ^{1}H NMR (400 MHz, DMSO-d_6): δ = 0.95–0.98 (3H, m, CH_3), 1.39–1.70 (10H, m, -CH_2-), 2.66–2.71 (2H, m, C=C*H*CH_2) and 6.35–6.39 (1H, m, C=C*H*).

4.2.54. (*Z*)-5-Decylidene-2-thioxothiazolidin-4-one (63)

Following *representative procedure 2*: *n*-decanal (188 μL, 1.00 mmol) was distilled and added to 2-thioxothiazolidin-4-one (0.133 g, 1.00 mmol) gave **63** (0.065 g, 24%) as a yellow solid; mp 74–76 °C; {lit.[63] mp 76–76.5 °C}; ^{1}H NMR (400 MHz, DMSO-d_6): δ = 0.92–0.95 (3H, m, CH_3), 1.32–1.70 (14H, m, —CH_2—), 2.66–2.71 (2H, m, C=CCHCH_2) and 6.36–6.42 (1H, m, C=C*H*).

4.2.55. (*Z*)-5-(1′-Phenylethylidene)-2-thioxothiazolidin-4-one (64)

Following *representative procedure 2*: acetophenone (0.120 g, 1.00 mmol) and 2-thioxothiazolidin-4-one (0.133 g, 1.00 mmol) gave **64** (0.265 g, 95%) as an orange solid; mp 207–209 °C; {lit.[63] mp 165–166 °C}; ^{1}H NMR (400 MHz, DMSO-d_6): δ = 2.58 (3H, s, C=CCH_3), 7.39–7.73 (3H, m, Ar*H*) and 7.90–8.04 (2H, m, Ar*H*).

4.2.56. (*Z*)-3-Methyl-5-(1′-phenylethylidene)-2-thioxothiazolidin-4-one (65)

Following *representative procedure 2*: acetophenone (0.120 g, 1.00 mmol) and 3-methyl-2-thioxothiazolidin-4-one (0.147 g, 1.00 mmol) gave **65** (0.218 g, 88%) as an orange solid; mp 169–170 °C; ^{1}H NMR (200 MHz, DMSO-d_6): δ = 2.58 (3H, s, $ArCH_3$), 3.32 (3H, s, NCH_3), 7.39–7.73 (3H, m, ArH) and 7.88–8.03 (2H, m, ArH and C=C*H*).

Acknowledgements

The authors acknowledge the Wellcome Trust for providing financial support, Research Councils UK for a fellowship (A.J.R.) and the MRC for a Chemical Biology Priority studentship (I.M.W.). Thanks are also due to Nathan Lack and Chan-Ju Wang for generating the Ligplot diagram. We thank Liz Fullam for supplying MMNAT.

References and notes

1. Sim, E.; Westwood, I.; Fullam, E. *Expert Opin. Drug Metab. Toxicol.* **2007**, *3*, 169.
2. Price Evans, D. A.; Manley, K. A.; McKusick, V. A. *Br. Med. J.* **1960**, *2*, 485.
3. Price Evans, D. A. *Pharmacol. Ther.* **1989**, *42*, 157.
4. http://louisville.edu/medschool/pharmacology/NAT.html.
5. Hein, D. W.; Boukouvala, S.; Grant, D. M.; Minchin, R. F.; Sim, E. *Pharmacogenet. Genomics* **2008**, *18*, 367.
6. Upton, A.; Johnson, N.; Sandy, J.; Sim, E. *Trends Pharmacol. Sci.* **2001**, *22*, 140.
7. Ohsako, S.; Deguchi, T. *J. Biol. Chem.* **1990**, *265*, 4630.
8. Blum, M.; Grant, D. M.; McBride, W.; Heim, M.; Meyer, U. A. *DNA Cell Biol.* **1990**, *9*, 193.
9. Riddle, B.; Jencks, W. P. *J. Biol. Chem.* **1971**, *246*, 3250.
10. Hein, D. W.; Doll, M. A.; Rustan, T. D.; Gray, K.; Feng, Y.; Ferguson, R. J.; Grant, D. M. *Carcinogenesis* **1993**, *14*, 1633.
11. Brooke, E. W.; Davies, S. G.; Mulvaney, A. W.; Pompeo, F.; Sim, E.; Vickers, R. J. *Bioorg. Med. Chem.* **2003**, *11*, 1227.
12. Hanna, P. E. *Adv. Pharmacol.* **1994**, *27*, 401.
13. Sinclair, J. C.; Sandy, J.; Delgoda, R.; Sim, E.; Noble, M. E. *Nat. Struct. Biol.* **2000**, *7*, 560.
14. Sandy, J.; Mushtaq, A.; Kawamura, A.; Sinclair, J.; Sim, E.; Noble, M. *J. Mol. Biol.* **2002**, *318*, 1071.
15. Westwood, I. M.; Holton, S. J.; Rodrigues-Lima, F.; Dupret, J. M.; Bhakta, S.; Noble, M. E.; Sim, E. *Biochem. J.* **2005**, *385*, 605.
16. Wu, H.; Dombrovsky, L.; Tempel, W.; Martin, F.; Loppnau, P.; Goodfellow, G. H.; Grant, D. M.; Plotnikov, A. N. *J. Biol. Chem.* **2007**, *282*, 30189.
17. Kawamura, A.; Graham, J.; Mushtaq, A.; Tsiftsoglou, S. A.; Vath, G. M.; Hanna, P. E.; Wagner, C. R.; Sim, E. *Biochem. Pharmacol.* **2005**, *69*, 347.
18. Grant, D. M.; Blum, M.; Beer, M.; Meyer, U. A. *Mol. Pharmacol.* **1991**, *39*, 184.
19. Hickman, D.; Palamanda, J. R.; Unadkat, J. D.; Sim, E. *Biochem. Pharmacol.* **1995**, *50*, 697.
20. Kawamura, A.; Westwood, I.; Wakefield, L.; Long, H.; Zhang, N.; Walters, K.; Redfield, C.; Sim, E. *Biochem. Pharmacol.* **2008**, *75*, 1550.
21. Hickman, D.; Pope, J.; Patil, S. D.; Fakis, G.; Smelt, V.; Stanley, L. A.; Payton, M.; Unadkat, J. D.; Sim, E. *Gut* **1998**, *42*, 402; Cribb, A. E.; Grant, D. M.; Miller, M. A.; Spielberg, S. P. *J. Pharmacol. Exp. Ther.* **1991**, *259*, 1241; Risch, A.; Smelt, V.; Lane, D.; Stanley, L.; van der Slot, W.; Ward, A.; Sim, E. *Pharmacol. Toxicol.* **1996**, *78*, 235; Stanley, L. A.; Coroneos, E.; Cuff, R.; Hickman, D.; Ward, A.; Sim, E. *J. Histochem. Cytochem.* **1996**, *44*, 1059.
22. McQueen, C. A.; Mitchell, M. K.; Dang, L. N.; Chau, B.; Tjalkens, R. B.; Philbert, M. A. *Chem. Biol. Interact.* **2003**, *145*, 77.
23. Boukouvala, S.; Fakis, G. *Drug Metab. Rev.* **2005**, *37*, 511–564.
24. Smelt, V. A.; Upton, A.; Adjaye, J.; Payton, M. A.; Boukouvala, S.; Johnson, N.; Mardon, H. J.; Sim, E. *Hum. Mol. Genet.* **2000**, *9*, 1101.
25. Stanley, L. A.; Copp, A. J.; Pope, J.; Rolls, S.; Smelt, V.; Perry, V. H.; Sim, E. *Teratology* **1998**, *58*, 174.
26. Wakefield, L.; Cornish, V.; Long, H.; Kawamura, A.; Zhang, X.; Hein, D. W.; Sim, E. *Biomarkers* **2008**, *13*, 106.
27. Richards, V. E.; Chau, B.; White, M. R.; McQueen, C. A. *Toxicol. Sci.* **2004**, *82*, 318.
28. Minchin, R. F. *Biochem. J.* **1995**, *307*, 1.
29. Wakefield, L.; Cornish, V.; Long, H.; Griffiths, W. J.; Sim, E. *Biochem. Biophys. Res. Commun.* **2007**, *364*, 556.
30. Tozlu, S.; Girault, I.; Vacher, S.; Vendrell, J.; Andrieu, C.; Spyratos, F.; Cohen, P.; Lidereau, R.; Bieche, I. *Endocr. Relat. Cancer.* **2006**, *13*, 1109.
31. Adam, P. J.; Berry, J.; Loader, J. A.; Tyson, K. L.; Craggs, G.; Smith, P.; De Belin, J.; Steers, G.; Pezzella, F.; Sachsenmeir, K. F.; Stamps, A. C.; Herath, A.; Sim, E.; O'Hare, M. J.; Harris, A. L.; Terrett, J. A. *Mol. Cancer Res.* **2003**, *1*, 826.
32. Bieche, I.; Girault, I.; Urbain, E.; Tozlu, S.; Lidereau, R. *Breast Cancer Res.* **2004**, *6*, R252.
33. Kim, Y. I. *Nutr. Rev.* **2006**, *64*, 468.
34. Kim, Y. I. *Mol. Nutr. Food Res.* **2007**, *51*, 267.
35. Heel, R. C.; Brogden, R. N.; Speight, T. M.; Avery, G. S. *Drugs* **1978**, *16*, 1.
36. Lee, J. H.; Chung, J. G.; Lai, J. M.; Levy, G. N.; Weber, W. W. *Cancer Lett.* **1997**, *111*, 39.
37. Lu, K. H.; Lin, K. L.; Hsia, T. C.; Hung, C. F.; Chou, M. C.; Hsiao, Y. M.; Chung, J. G. *Res. Commun. Mol. Pathol. Pharmacol.* **2001**, *109*, 319; Lee, J. H.; Lu, H. F.; Wang, D. Y.; Chen, D. R.; Su, C. C.; Chen, Y. S.; Yang, J. H.; Chung, J. G. *Res. Commun. Mol. Pathol. Pharmacol.* **2004**, *115*(116), 217.
38. Ragunathan, N.; Dairou, J.; Pluvinage, B.; Martins, M.; Petit, E.; Janel, N.; Dupret, J.-M.; Rodrigues-Lima, F. *Mol. Pharmacol.* **2008**, *73*, 1761.
39. Zhu, Y.; Wang, A.; Liu, M. C.; Zwart, A.; Lee, R. Y.; Gallagher, A.; Wang, Y.; Miller, W. R.; Dixon, J. M.; Clarke, R. *Int. J. Oncol.* **2006**, *29*, 1581.
40. Wakefield, L.; Robinson, J.; Long, H.; Ibbitt, J. C.; Cooke, S.; Hurst, H. C.; Sim, E. *Genes Chromosomes Cancer* **2008**, *47*, 118.
41. Miller, L. D.; Smeds, J.; George, J.; Vega, V. B.; Vergara, L.; Ploner, A.; Pawitan, Y.; Hall, P.; Klaar, S.; Liu, E. T.; Bergh, J. *Proc. Natl. Acad. Sci. U.S.A.* **2005**, *102*, 13550.
42. http://info.cancerresearchuk.org/cancerstats/types/breast/incidence/.
43. Weinshilboum, R.. In *Advances in Experimental Medicine and Biology*; Berstein, L. M., Santen, R. J., Eds.; Plenum Press: New York and London, 2008; Vol. 630, p 220.
44. Voice, R. A.; Manis, M.; Weber, W. W. *Drug Metabol. Dispos.* **1993**, *21*, 181; Wang, H.; Vath, G. M.; Gleason, K. J.; Hanna, P. E.; Wagner, C. R. *Biochemistry* **2004**, *43*, 8234; Cheon, H. G.; Hanna, P. E. *Biochem. Pharmacol.* **1992**, *43*, 2255; Cheon, H. G.; Boteju, L. W.; Hanna, P. E. *Mol. Pharmacol.* **1992**, *42*, 82; Guo, Z.; Wagner, C. R.; Hanna, P. E. *Chem. Res. Toxicol.* **2004**, *17*, 275; Sticha, K. R.; Bergstrom, C. P.; Wagner, C. R.; Hanna, P. E. *Biochem. Pharmacol.* **1998**, *56*, 47; Wang, H.; Wagner, C. R.; Hanna, P. E. *Chem. Res. Toxicol.* **2005**, *18*, 183; Wang, H.; Guo, Z.; Vath, G. M.; Wagner, C. R.; Hanna, P. E. *Protein J.* **2004**, *23*, 153; Dairou, J.; Atmane, N.; Dupret, J. M.; Rodrigues-Lima, F. *Biochem. Biophys. Res. Commun.* **2003**, *307*, 1059; Dairou, J.; Atmane, N.; Rodrigues-Lima, F.; Dupret, J. M. *J. Biol. Chem.* **2004**, *279*, 7708.
45. Westwood, I. M.; Kawamura, A.; Fullam, E.; Russell, A. J.; Davies, S. G.; Sim, E. *Curr. Top. Med. Chem.* **2006**, *6*, 1641; Brooke, E. W.; Davies, S. G.; Mulvaney, A. W.; Okada, M.; Pompeo, F.; Sim, E.; Vickers, R. J.; Westwood, I. M. *Bioorg. Med. Chem. Lett.* **2003**, *13*, 2527.
46. Kawamura, A., D.Phil Thesis, University of Oxford, 2004; Westwood, I. M., D.Phil Thesis, University of Oxford, 2005.
47. Wang, H.; Vath, G. M.; Kawamura, A.; Bates, C. A.; Sim, E.; Hanna, P. E.; Wagner, C. R. *Protein J.* **2005**, *24*, 55.
48. Sinclair, J. C.; Delgoda, R.; Noble, M. E.; Jarmin, S.; Goh, N. K.; Sim, E. *Protein Expr. Purif.* **1998**, *12*, 371.
49. Lipinski, C. A.; Lombardo, F.; Dominy, B. W.; Feeney, P. J. *Adv. Drug Deliv. Rev.* **2001**, *46*, 3.
50. Westwood, I. M.; Sim, E. *BMC Biochem.* **2007**, *8*, 3; Mushtaq, A.; Payton, M.; Sim, E. *J. Biol. Chem.* **2002**, *277*, 12175.
51. Fullam, E.; Westwood, I. M.; Anderton, M. C.; Lowe, E. D.; Sim, E.; Noble, M. E. M. *J. Mol. Biol.* **2008**, *375*, 178.
52. Song, Y.; Connor, D. T.; Doubleday, R.; Sorenson, R. J.; Sercel, A. D.; Unangst, P. C.; Roth, B. D.; Gilbertson, R. B.; Chan, K.; Schrier, D. J.; Guglietta, A.; Bornemeier, D. A.; Dyer, R. D. *J. Med. Chem.* **1999**, *42*, 1151.
53. Kandeel, K. A. *Chem. Pap.* **2004**, *58*, 334.
54. Congreve, M.; Chessari, G.; Tisi, D.; Woodhead, A. J. *J. Med. Chem.* **2008**, *51*, 3661.
55. Morris, G. M.; Goodsell, D. S.; Halliday, R. S.; Huey, R.; Hart, W. E.; Belew, R. K.; Olson, A. J. *J. Comput. Chem.* **1998**, *19*, 1639; Goodsell, D. S.; Morris, G. M.; Olson, A. J. *J. Mol. Recogn.* **1996**, *9*, 1.
56. Verdonk, M. L.; Cole, J. C.; Hartshorn, M. J.; Murray, C. W.; Taylor, R. D. *Proteins* **2003**, *52*, 609.
57. Pettersen, E. F.; Goddard, T. D.; Huang, C. C.; Couch, G. S.; Greenblatt, D. M.; Meng, E. C.; Ferrin, T. E. *J. Comput. Chem.* **2004**, *25*, 1605.
58. Holton, S. J.; Dairou, J.; Sandy, J.; Rodrigues-Lima, F.; Dupret, J. M.; Noble, M. E. M.; Sim, E. *Acta Crystallogr. F* **2005**, *61*, 14.
59. Pangborn, A. B.; Giardello, M. A.; Grubbs, R. H.; Rosen, R. K.; Timmers, F. J. *Organometallics* **1996**, *15*, 1518.
60. Prashantha Kumar, B. R.; Karvekar, M. D.; Adhikary, L.; Nanjan, M. J.; Suresh, B. *J. Heterocycl. Chem.* **2006**, *43*, 897.
61. Ravazzoni, V. *Ann. Chim.* **1962**, *52*, 305.
62. Groves, L. H.; Swan, G. A. *J. Chem. Soc.* **1952**, 650.
63. Brown, F. C.; Bradsher, C. K.; Bond, S. M.; Potter, M. *J. Am. Chem. Soc.* **1951**, *73*, 2357.
64. Podkoscielny, W. *Phys. Chem.* **1975**, *29*, 289.
65. Unangst, P. C.; Connor, D. T.; Cetenko, W. A.; Sorenson, R. J.; Kostlan, C. R.; Sircar, J. C.; Wright, C. D.; Schrier, D. J.; Dyer, R. D. *J. Med. Chem.* **1994**, *37*, 322.
66. Andreasch, R.; Zipser, A. *Monatsh. Chem.* **1904**, *25*, 159.
67. Omar, M. T. S. *J. Prakt. Chem.* **1980**, *5*, 835.
68. Sortino, M.; Delgado, P.; Juárez, S.; Quiroga, J.; Abon?a, R.; Insuasty, B.; Nogueras, M.; Rodero, L.; Garibotto, F. M.; Enriz, R. D.; Zacchino, S. A. *Bioorg. Med. Chem.* **2007**, *15*, 484.
69. Bradsher, C. K.; Kittila, R. S. *J. Org. Chem.* **1950**, *15*, 374.
70. Bourahla, K.; Derdour, A.; Rahmouni, M.; Carreaux, F.; Bazureau, J. P. *Tetrahedron Lett.* **2007**, *48*, 5785.
71. Ilan, F. J. A.; Graham, G.; Thomson, J. B. *Can. J. Chem.* **1958**, *36*, 1579.
72. Lugovkin, B. P. *J. Gen. Chem. U.S.S.R.* **1971**, *41*, 821.